Preferred citation: J.-F. Bloch and S. Rolland du Roscoat. Review: Three-dimensional structural analysis. In **Advances in Pulp and Paper Research, Oxford 2009**, *Trans. of the XIVth Fund. Res. Symp. Oxford, 2009*, (S.J. I'Anson, ed.), pp 599–664, FRC, Manchester, 2018. DOI: 10.15376/frc.2009.2.599.

THREE-DIMENSIONAL STRUCTURAL ANALYSIS

Jean-Francis Bloch[1] *and Sabine Rolland du Roscoat*[2]

[1]G-INP/Pagora/LGP2/CNRS BP 65 F38402 Saint Martin d'Hères, France
[2]UJF/3S-R/CNRS, BP 53, F-38041, Grenoble Cedex 9, France

ABSTRACT

The literature related to the three-dimensional fibre networks is reviewed since 2000. Indeed, a review was presented in these symposia in 2001 [1]. Therefore, the updated articles are only considered here. The previous review concentrated on theory, whereas the focus here is on modern 3D analysis and comparisons of these with theory. Moreover, the focus is on paper structure. However, the general context of 3D structure is considered in the introduction in order to illustrate the main ideas that may be applied to paper. Then, the experimental methods are presented in order to show the potential of such techniques. In a third part, improvements of the description of the 3D structure will be presented. Namely, the quantitative description that completes the visualisation of the structures will be presented. The main 3D morphological properties will be presented and some examples will illustrate the existing developed tools. The Representative Elementary Volume (REV) dedicated to the structure properties will then be introduced. The theoretical models are briefly presented to prove the necessary development of both experimental tools and dedicated theories. Theoretical studies will be exemplified. Indeed, both theoretical and experimental demarches will enrich each other as will be shown. The influence of both deformation and humidity modifications on the 3D structure will illustrate the interest of the knowledge of the 3D structure, to tackle its influence on physical properties. The main perspectives and challenges related to the structure description will end up this presentation.

OUTLINE

INTRODUCTION

Context of the review

The presentation is dedicated to the fabrication of paper. Hence, the discussion will be oriented towards this particular application, having in mind other materials. The context of this contribution is that two very interesting papers have already been published in this conference. The first one appeared in 1962 [2] completed by numerous articles published in the sixties. The more recent consists in a review, by Sampson, and was published in 2001 [1]. Furthermore, his book [3] published is a scientific basis to study the fibrous structure of paper and practise in numerical simulation. It represents a complementary approach to the earlier book of Dodson [4]. Many references are provided in these publications. The aim here is not to review these reviews, instead it is to present the progress since 2000. Furthermore, it is not within the scope of this paper to review the literature relating the structure to end-use physical properties, even though it is obviously the main objective of the structure description. Moreover, there exist different books that present mathematical analyses of microstructure and the macroscopic properties [5,6]. The aim here is a three-dimensional description of the microstructure of paper, so we focus only on this, considering both complementary theoretical and experimental points of view. We will underline the experimental aspects, as the theoretical aspects are well described elsewhere as mentioned before. Finally, we also would like to emphasise the complementary role of both the theoretical aspects and experimental developments.

3D structure of materials

Classical structural characterisations are often carried out on 2D data sets. This is however not sufficient to describe properly for example the fibrous or porous network connectivity. Therefore, since few decades, efforts have been made to visualise and analyse in 3D the inner material. It was applied for example to study the bone structure [7,8] or relative permeability of porous materials [9]. Even though the paper is not included in the studied materials, El Raoush [10] published the following interesting table, including both the experimental technique and the structural parameters showing the potential of 3D measurements.

Increasing demands exist nowadays concerning the faithful visualisation of the 3D structure of paper, and these carry forward to the accurate quantification of structural parameters. The developments are also nowadays possible due to the new numerical calculation abilities and accurate technologies applied in measurement equipment. Namely, laboratory equipments allowing

Table 1. Applications of imaging techniques to porous media systems [10].

Reference	*System*	*Resolution*	*Porous media*	*Measured properties*
Petrovic and *et al.* (1982)	X-ray scanner	*	Soil, glass beads	Soil bulk density
Crestana and *et al.* (1985)	X-ray computed tomography	*	Sandy and fine sandy loam	Water content variations
Crestana and *et al.* (1986)	X-ray mini scanner	*	Fine sandy loam	Water content and soil bulk/density
Harold and *et al.* (1987)	X-ray computed tomography	*	Bera sandstone	Volume fractions
Hunt and *et al.* (1988)	X-ray computed tomography	*	Natural soil	Fractures, mud invasion, and litholgic characterization
Warner and *et al.* (1989)	X-ray computed tomography	*	Natural soil	Air filled porosity and pore size distribution
Cassel and *et al.* (1990)	X-ray computed tomography	*	Natural soil	Variation in water content
Spanne and *et al.* (1994)	Synchrotron computed tomography	10 mm	Fontainebleau sandstone	Topology and connectivity
Montemagno and Gray, (1995)	Photoluminescence volumetric imaging	1 mm	Random soil samples	Porosity, volume fractions and specific surface area
Auzerais and *et al.* (1996)	X-ray computed tomography	7.5 mm	Fontainebleau sandstone	Porosity, volume fractions, permeability and connectivity
Coker and Torquato (1996)	Synchrotron tomography	7.5 mm	Fontainebleau sandstone	Porosity, specific surface area and pore size distribution
Lindquist and Lee (1996)	X-ray computed tomography	5 mm	Bera sandstone, glass bead	Porosity, tortuosity, connectivity and specific surface area

Table 1. Continued

Reference	*System*	*Resolution*	*Porous media*	*Measured properties*
Baldwin and *et al.* (1996)	Magnetic Resonance Imaging	*	Uniform glass beads	Pore size distribution, coordination, and specific surface area
Pauli and *et al.* (1997)	Magnetic Resonance Imaging	*	Glass filter system	Pore size distribution
Klobes and *et al.* (1997)	X ray computed tomography with mercury porosimetry	400 mm	Rock samples	Porosity
Kahalili and *et al.* (1998)	Positron emission tomography	*	Sandy sediment soil	Visualization of fluid transport through the sample
Coles and *et al.* (1998)	Synchrotron tomography	30 mm	Sandstone	Porosity and water content
Hsieh and *et al.* (1998)	Gamma-ray computed tomography	*	Dolomite Porosity and volume fractions	
Clausuitzer and Hopmans (1999)	X ray computed tomography	*	Glass beads	Volume fractions
Lindquist and Venkatarangan (1999)	Synchrotron tomography	6 mm	Fontainebleau sandstone	Geometrical analysis
Khalili and *et al.* (1998)	Positron emission tomography	*	Sandy sediment soil	Visualization of fluid transport through the sample
Solymar and Fabricius (1999)	Scanning electron microscopy	1.6 mm	Silty and clayey quartz	Porosity, permeability, and specific surface area
Wildenscheld and *et al.* (2002)	Various	Various	Glass Beads	Porosity, volumetric water content

* *Resolution is of the order of mm or not provided by the author.*

3D visualisation of inner structure have dramatically increased in the past five years. These complement the possibilities offered by the so-called large instruments such as Swiss Light Source (SLS), European Synchrotron Radiation Facility (ESRF) or Argonne Advanced Photon Source (APS). Moreover, different devices may also be coupled offering new perspectives by carrying out mechanical in situ test for example. Therefore, to complete the qualitative analysis, active developments of algorithmic tools aimed at image analysis, such as segmentation, recognition, or deformation estimation, have been developed recently and are undergoing continued refinement and development. However, we have often suffered from insufficient dialogue between scientists from different fields, or due to a fear of competition, which in fact may lead to a healthy concurrence or competition. However, the main improvements have, and will be based on the ability to establish well-posed questions from both fundamental and experimental objectives. In this way, the capabilities to extract, quantify and/or interpret the structural information directly impact on the ability to feed, validate or even build relevant models. In the paper industrial context, the variation of the raw materials, the variability of disorder appearance at different scales of observation, the inaccuracies or the uncertainties in either measurements or even theories, constitute our every day scientific life. We have to deal with these aspects. The latest technological improvements allow obtaining many measures of different properties dedicated to almost any studied physical problem taken into consideration into regions representing meaningful objects. Hence, for example, the definition and evaluation of the Representative Elementary Volume (REV) is a prerequisite to develop understanding in paper science. Naturally, this volume does depend on the physical properties of interest. This will lead to the necessary framework of the next development steps. Furthermore, the characteristic length and time have to be explicitly considered for any physical analysis. It will help develop the crucial dialogue between scientists. An example is the increasing interest concerning the bridge between fibres and higher levels of organisation, such as either microstructure or at the formation scales. However, the solution of this inter-level processes, relies on information on both the structure and the functional aspects.

Furthermore, the arbitrary distinction between the bulk and the surface properties may be discussed. The objects or structure close to the surface may be imaged directly by confocal microscopy for example. If the depth information is investigated, other methods such as microtomy or microtomography are necessary.

Quantification of parameters is the current aim of research, associated sometimes with an estimation of the influence of process parameters. To exemplify this, we may indicate the shape, position, and deformation of the

components of paper structures. The objective is here to define and quantify adequate structural parameters that are supposed to fully define them and eventually to establish their relationships. However, as claimed before, different scales exist in the paper structure, as well presented by Kortschot [11] in a previous conference. Usually, we start from a given scale looking, through an up scaling technique, to obtain a description at the 'macroscopic' scale. The main difficulty is here often to consider multi-physical problems, which couple the effects, eventually in a non linear way. In this context, the experimental data and/or models may lead to point out the missing elements, whatever they are, ensuring the coherence of the explanation of the observed physical phenomena. Of course, we have to bear in mind that the final aims are to increase the efficiency of the paper industry.

Models or experiments?

Models may be, in a way, considered as a predictive science. They may also be used to establish the best way to plan experiments and trials. Moreover, models help not only in obtaining a description but may also have an interest in providing solutions to the studied problem. One may expect that they improve the resolution of a problem by introducing either explicit or implicit current knowledge to the reasoning. They may help also to modify or explain some 'industrial internal recipes' or explain their limitations, such as their domain of validity. Many models exist such as ones based on physical knowledge, grey- or black-box models. Any approaches that may be useful, have to be introduced, even at different stages such as control or diagnosis. In our context, we are often more attracted to the knowledge based approach, but we have to be open to others. Furthermore, numerical approaches may be used either to compare different theories or to illustrate them. It appears frequently nowadays that we are carrying out 'numerical' studies to estimate the influence of a given parameter. This may help to test the sensitivity of the model to a parameter and its robustness. Numerical simulations contribute also to key research issues as they may be used either in direct or inverse problems. In order to rephrase this idea, we may use a model to elaborate a given structure *ab initio* and then evaluate the physical properties from the obtained structure (this is not in the scope of this paper, but will be illustrated in this conference) or use macroscopic physical properties to estimate the structural parameters. Inverse problems are often used in an implicit way. A classical example may be given: from the porosity and the specific surface, the permeability may be estimated, using for example the Kozeny-Carman relation. Or, from the knowledge of the flow through the fibrous structure, we may estimate structural properties. As an illustration, we may cite the works

of Jaganathan and *et al.* [12,13] or that presented in this conference by Koivu and *et al.* [14]. The introduction of topology may be important also when considering, for example, the permeability, as illustrated in [9]. Both are of major interest for paper scientists. Simulation relies on a proposed model of different mechanisms to be studied and its first goal is to realistically reproduce the observed (or assumed) behaviours. Such mathematical descriptions aim to improve our understanding not necessary to be used in an explanation context. In this way, they also may be considered as a first, or complementary, step of experiences on real data. Furthermore, they may be useful to assess to results of virtual experiences that are not possible for technical reason. For example, if we analyse the influence of fibre morphology on structure of paper, it is almost impossible in a practical context to decouple each of the physical parameters that are well known to play a role, such as fibre length, coarseness, width or diameter. Using a model, each parameter may be modified independently and its influence studied.

A lot of progress is required in order to estimate the final end use properties of a paper sheet from the introduction of fibres either in the refiner or at the head box. As it is well known the drying conditions, for example, play a major role in the mechanical properties. And this is true for any unit operations of paper manufacture. The studied system and/or material are quite complex and the observable variables are often sparse or even not directly measurable. In this way, simulations either of the fibrous structure or of its physical properties may be introduced to predict or control the process. Furthermore, Torquato [6,15] stated that the topology has to be introduced if an optimisation method is introduced, in order to *'distribute a given amount of material in a design domain such that an objective function is extremized'*. Levitz [16] introduced two strategies to tackle the 3D modeling:

– '*Simulate or mimic the physical and chemical processes, and to compare the result with the available experimental geometrical information*'. It is often a case by case analysis but it provides a good understanding of the physical phenomena considered.
– '*Perform a 3D reconstruction of the material from limited but relatively accurate structural information*'.

The measure of the 3D structure of paper will be useful and complementary in both strategies. Consequently, models may be used to find the most sensitive parameters and to compare the outputs to the observations. Also, from an industrial point of view, the hope is to be able to stabilise the industrial process that is to say to revert to normal conditions by establishing model parameter deviations from normal behaviours. In other words, the aim is to study the influence of the modification of either the mean value of a

parameter or considering its standard deviation. The tendency was also to generate model of the network, either from a model or based on microtomography information. For example, we may refer to [17] and the interesting references included. They need to introduce pore-pore correlations and so-called pore-throat correlations in order to avoid obtaining what they call a 'poor representation'. They claim that in the past, '*microstructure has been limited to oversimplified representations of the structure*'. Furthermore, if the percolation concept has to be introduced, '*there is an urgent need to generate stochastic network based structures representative of their complexity*'. Basic mechanisms and their interaction have been studied since a long time. However, the road is still long as they involve a huge number of variables influencing the 3D structure at different levels of organisation. The necessary, but limited at long term, accumulation of individual (in the sense of unique) field of concern will necessary have a poor impact. Non linearities, couplings, for example, have to be introduced. To illustrate this idea, the mechanical properties have been studied for decades, as has the influence of humidity on structure. However, one aim remains a full study of mechanical behaviour including humidity variations. It is of course a simple illustration, but a necessary one. The classical and necessary method consists in first the description of the studied physics at each necessary scales and further, by modelling the interactions of the physical chosen variables to obtain a so called 'macroscopic' model. Then, and only then, a better understanding of the studied processes may emerged. That is to say we have to find a scientific path from the microscopic description to the corresponding global macroscopic properties at a higher level of organisation. As cited before, Kortschot [11] introduced in this Conference, in 1997, the hierarchical concept applied to paper. He also presented the physical variables which influence the fibrous network, namely, the fiber strength, the specific bond strength, the light absorption coefficient, the fiber length the fiber coarseness, the relative bond area and the fiber width. In this way, we will see that the fiber width is a fundamental property if the microstructure is considered. As it has been understood since the beginning of paper physics, the individual models of the constructive elements may differ from the one of the assemblies of such elementary elements. Furthermore, the physical description of a given physical phenomena may have to be different. To illustrate briefly this, the local description of the flow at the micro-scale may be tackled using the Navier-Stokes equation, but at the macroscopic scale the structure of the law is different, namely the well-known Darcy law.

Torquato [6,18,19] stated that *'Empirical relations are more useful for correlating data rather than predicting them. Since effective properties are sensitive to the details of the microstructure, a broader approach is to calculate the*

properties from the microstructure of the disordered materials; one can then relate changes in the microstructure quantitatively to changes in the macroscopic parameters. This has important implications for the design of materials with tailored properties'.

Consequently, the development of models as such, is necessary but not enough. It has to be confronted to experiments. Moreover, the explanation of simple properties, and their inherent assumptions about structures and their evolution, associated to data, may lead to better prediction or decision capabilities. However, the scientists have also to check that their knowledge is either introduced in such approach or compatible with it.

Finally, in order to obtain the reached 'breakthrough' that are required, efforts have to continue on theoretical aspects, model developments, numerical simulations and experimental set-ups, data collecting and quantification. Figure 1 illustrates the main interests of the scientific community involved in this long term research.

In such a context, the aim of this paper is to present some experimental tools that are nowadays able to describe the 3D microstructure of papers at a chosen scale and then to check that the quantified descriptors of this structure may be related to the proposed models found in the literature dedicated to the structure of fibrous materials. The coated papers are not on the scope of this presentation. The reader may refer to ([20], [21]), for example.

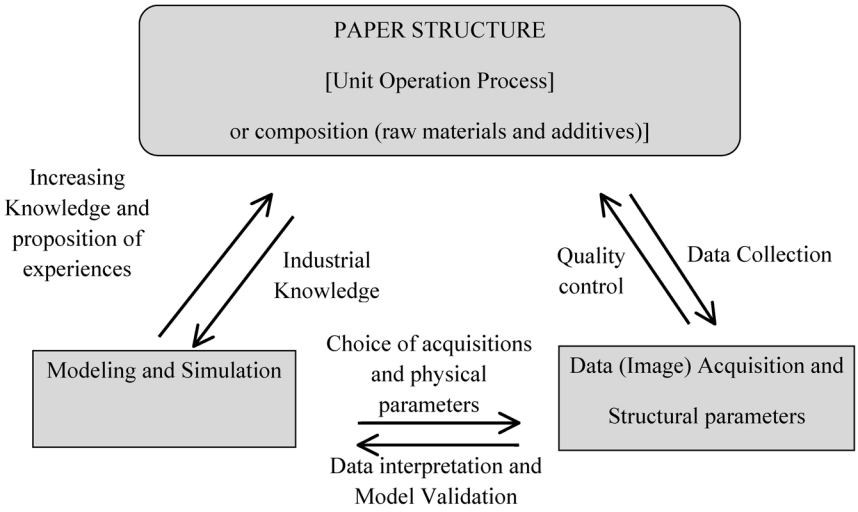

Figure 1. Schematic description of the interrelations between the 3D structure of paper, the model development and the process influences.

The description of the experimental equipments, the current (and future) structural properties is here underlined. In particular, we will mention essentially the microtome approach and the X-Ray microtomography, as they represent the best illustrations, in the context of this presentation. For example, the number of communications dedicated to X-ray microtomography (3d data set visualisation and quantification, numerical estimation of physical properties on 3D data set . . .) is still increasing as shown in Figure 2 (the data were obtained from a research on ISI Web of Knowledge).

To conclude this introduction, we cite Knackstedt and *et al.*, [22] who developed a very interesting concept while dealing with tomographic data: a virtual material laboratory. He summarised clearly the new scientific trend: '*Tomographic imaging can now be routinely performed over three orders of magnitude in length scale with corresponding high data quality. This capability, coupled with the development of advanced computational algorithms for image interpretation, three-dimensional visualization, and structural characterization and computation of physical properties on image data, allows for a new laboratory approach to the study of real complex media*'. It is obvious that paper is a perfect example of such a concept.

3D EXPERIMENTAL TECHNIQUES

The main techniques used experimentally to visualise the 3D structure of paper are briefly presented. Namely, confocal microscopy, the microtome coupled with an imaging system, optical tomography and finally X-ray micro-tomography will be considered. We will detail the last one, as it will be

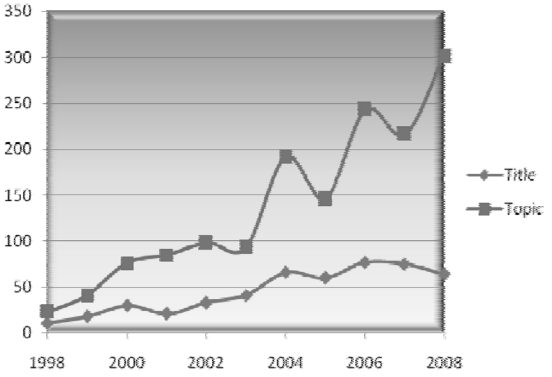

Figure 2. Number of Publications (Title or Topic) dedicated to X-Ray Microtomography vs. year (1998–2008).

the basis of the presentation. The interested reader may refer to [24], for example, for complementary description of experimental tools and to [25] in the case of the 3D description of paper. As claimed by Dobrich [23], '*properties of a material are determined largely by its microstructure. Although a great deal of information can be achieved from 2D techniques, (such as optical or Scanning Electron microscopy), there are a number of micro-structural features that can be ascertained adequately only via a truly 3D characterisation procedure*'. As an illustration, the connectivity of the fibrous network may be introduced.

Confocal microscopy

This instrument gives information on a plane inside the sample by optically sectioning it. A laser beam is focused on the analysed sample. The reflected light is then detected. A three dimensional data set can be obtained by varying the focal plane. The first results obtained for paper with this technique were reported in [26]. Unfortunately, such a device does not allow scanning the depth of paper as the intensity signal decreases rapidly when a deeper plane in the paper is investigated.

Microtome coupled with an imaging system

This method consists in sectioning in a given direction the samples and in imaging each successive section. The visualisation is carried out imaging each section with either an optical microscope or with a scanning electron microscope. This technique was used to study paper sample structure in the thickness direction for example in the PhD of Aronsson [27] or by Niskanen and Rajatora [28]. When gathering different sections, this method allows a 3D analysis of the paper structure. It has to be noted the recent advances in data acquisition, in particular the ease and speed of serial sectioning studies. To obtain an automatic tool, Wiltsche [25] during his PhD developed successfully an automatic system that consists in a light-optical microscope coupled with a microtome. The pixel size can be down to 0.16 μm which allows the detailed investigation of a coating layer for example. His description of destructive and non destructive methods is particularly didactic. The interested reader should refer to his presentation. This technique presents the advantage to be a laboratory equipment. The field of view is huge in comparison to other techniques. However, in such techniques, the preparation of the sample is crucial. Indeed, to be cut off, the samples must be embedded in a matrix which may modify the structure. The sectioning also requires the concatenation of the series of slices which is time consuming and requires

specific skills as mentioned in the works by Aronsson [27,29] and Witlsche [25,30]. However, this equipment constitutes an interesting experimental tool to obtain a detailed microstructure of a paper.

Optical tomography

Optical coherence tomography can also be applied to characterise the 3D paper structure as presented for example by Alarousu [31]. This technique uses low-coherence interferometry to produce a two-dimensional image of optical scattering from paper structure. By varying the different parameters of the interferometer, a succession of slices in the thickness can be recorded every 1–2 μm. It has been successfully used to visualise the outer layers of paper. However a detailed analysis of paper structure using such a technique seems not to be possible nowadays as the quality of the image seems not to be sufficient. This technique was also associated [32] with X-Ray Micro-tomography, presented hereafter.

X-ray Microtomography (XRM)

X-ray Microtomography allows one to get a 3D visualisation of the inner structure of the samples at a given scale (in the micrometer range). This method presents the advantages to be non-invasive and 'non destructive', that is to say few experiments on the same sample may be carried out. Here we briefly recall the principle of XRM. The analysed sample is set on a rotation plate. The sample is irradiated by an X-Ray beam. The transmitted beam is recorded for several angular projections. A filterbackprojection algorithm is then applied on the obtained 2D images to reconstruct the whole volume. Most of the results obtained on paper samples were acquired on the beamline ID19 at ESRF. More details on microtomography can be found in [33,34].

XRM may be performed either with a laboratory or a synchrotron source. First samples of paper were imaged on a Laboratory Tomograph in USA [35] and are currently performed at Jyväskylä University. First paper samples were visualised at ESRF in phase contrast mode by Samuelsen [36–38] and in absorption mode by Reverdy-Bruas [39,40]. The pixel sizes were 0.35 μm and 6 μm, respectively. As 6 microns was obviously not enough to obtain a detailed description of the structure the following tests were then carried out choosing a pixel size of 2 microns. Such a high pixel size gives an overview of the possibilities of this technique. It is obvious that the choice of the pixel size does depend both on the constituent's characteristic sizes, the experimental setup available and the aim of the description in term of Representative Elementary Volume. This aspect will be discussed in a next paragraph.

The images presented in Figure 3 exemplified the importance of the pixel size. The first was imaged with a pixel size of 1.9 μm by Reverdy in her PhD [40] and the second is imaged with a pixel size of 0.7 μm by Rolland du Roscoat [41].

Visual comparison of these two slices reveals differences in terms of a detailed description. We can easily distinguish the fibres on the right image whereas this is not the case in the left one. This is coherent with the conclusion made by Holmstad [42] in his comparison of high and low resolution. According to the typical sizes of paper constituents, a pixel size smaller than 1 micron is required. Indeed, the characteristic sizes of the constituents of paper are 30 microns for fibre diameter and 1 micron for filler. Due to the necessary equilibrium between the visual field of view and the necessary accuracy, the 0.7 pixel size is often used nowadays which leads to an imaged volume of (1.4 mm × 1.4 mm × paper_thickness). It should be noticed at this point that in the case of paper samples, synchrotron sources are required to produce images of high quality in term of signal to noise ratio and shape definition. The comparison made by Axelsson [43] illustrates this aspect on a board sample as seen in Figure 4.

We may note that in the context of paper making, Thibault [44,45] used also the absorption technique at ESRF for the visualisation of felts, involving a pixel size of 5 microns. He also visualised the 3D structure considering its

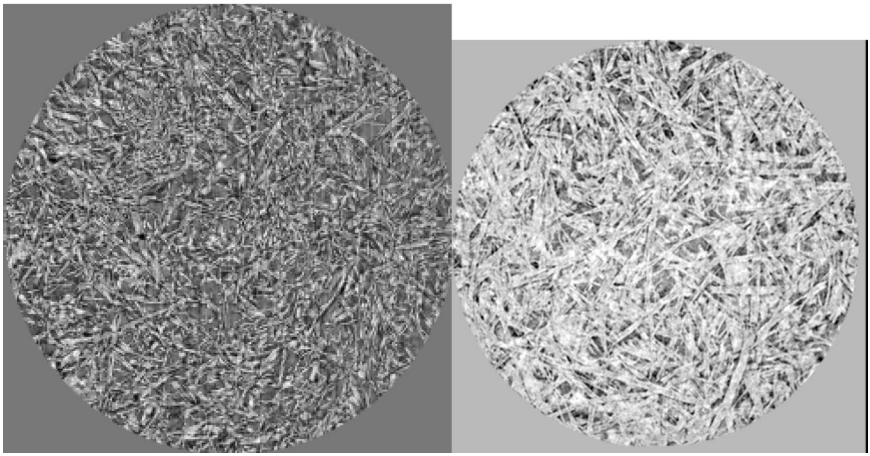

Figure 3. Influence of pixel size: The left slice (1.9 mm × 1.9 mm) represents an image at a pixel size of 1.9 μm. The right one (1.4 mm × 1.4 mm) represents another image at a pixel size of 0.7 μm. The scale is the same for both samples.

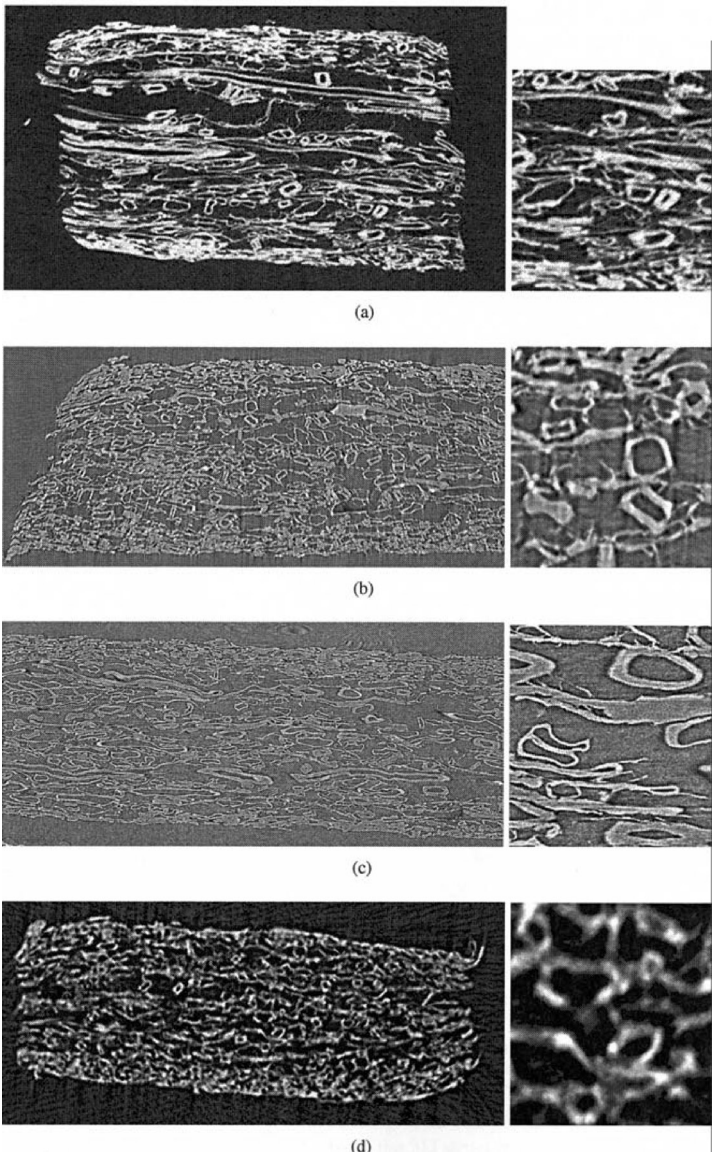

Figure 4. Images from four X-ray microtomography data set of a layered cardboard with a 200 × 200 pixel detail of each image (a) HASYLAB BW2 (1 pixel = 1.44 μm), (b) PSI Tomcat (1 pixel = 0.7 μm) (c) ESRF ID 19 (1 pixel = 0.7 μm) and (d) SKYSCAN 1172 (1 pixel = 0.78 μm) [43].

deformed structure. More recently, some forming fabrics have also been analysed using XRM in absorption at a pixel size of 5 microns [46].

We would like to mention the numerous works carried out nowadays on microtomographic data set of paper. Indeed, few PhD Thesis were recently dedicated to the analysis of the data obtained from microtomography. We may cite for example Holmstad (Norway), Defrennes (US), Turpeinen, Koivu (Finland), Aronsson, Axelsson (Sweden), Rolland du Roscoat, Decain, Viguié, Peralba (France). This not exhaustive list proves the interesting aspects of this technique which bridges the academic research to industrial investigations.

FROM VISUALISATION TO QUANTIFICATION

3D visualisation

First, Figure 5 exemplifies 3D visualisations of paper structures. It does concern four so-called 'reference papers', briefly presented hereafter:

– paper 'hard': Isotropic hand-sheet made of 100% of hardwood fibers, (thickness : 109 μm; basis weight: 67 g.m^{-2})
– paper 'blot': Industrial blotting paper, made of a mix of softwood and hardwood fibers, (thickness : 473 μm; basis weight: 246 g.m^{-2})

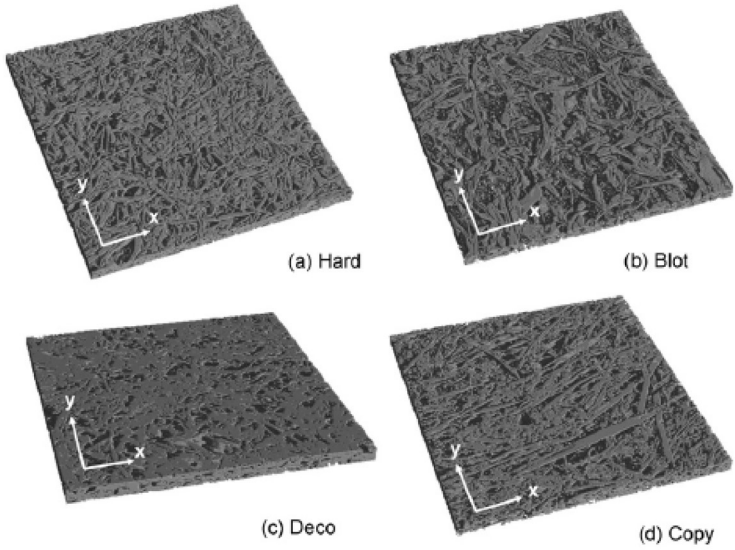

Figure 5. 3D visualisations of the reference papers (700 μm × 700 μm × 35 μm) [47].

– paper 'deco': Industrial decorative paper constituted of a mix of softwood and hardwood fibers, and filled with 35% to 40% of TiO_2, (thickness : 97 μm; basis weight: 85 $g.m^{-2}$)
– paper 'copy': it is an industrial printing paper. It contains different fibers (softwood, hardwood, recycled fibres) and fillers (around 20% of precipitated $CaCO_3$) (thickness: 111 μm; basis weight: 80 $g.m^{-2}$).

A brief qualitative description of the samples is first summarized. For the hardwood handsheet, no preferential anisotropy appears in the plane. If we are interested in porosity characterisation, then we can observe the large scale of porosity between the blotting paper and the decorative paper. Dealing with fibres, we can observe on the 'copy' paper, the long softwood fibres. Their structures seem to be quasi-isotropic in the plane direction due to the presence of fillers. From a visual point of view, all the samples seem to have an isotropic transverse structure (anisotropy in the thickness direction).

Methods of phase classification

The XRM data are obtained in grey levels which can be linked to the chemical composition of the samples. This is adapted for a visual and qualitative analysis. However, to quantify the structures, to compare them with theoretical models or to use them as input of numerical estimation, the separation of the different phases is required. To achieve an accurate segmentation, classical steps of any image processing chain are followed: filtering and segmentation. Two main approaches of segmentation are routinely used in the case of paper samples once the data are filtered. Both methods are implemented in 3D. The first one consists of adaptative thresholding techniques which allow the separation of the solid phase from the porous one. It was commonly used ([43], [48], [49]). This presents the advantage of being easy and quick, but it has the drawback of not being usable to isolate the fillers. The second one consists of using growing region techniques [33]. It presents the drawback of being more computationally intensive, but provides the advantage of isolating fillers. Furthermore it does not require user intervention, which was the aim, as previously claimed in [50]. Indeed in their case, they develop methods involving the intervention of the user in order to segment the image.

Example of application of the segmentation process: filler extraction

The fillers are generally more absorbent to X-Ray than fibres and can be observed at a pixel size of 0.7 μm. In order to obtain quantitative measurements, they have to be separated from the pores and the fibres. In this scope, the developed segmentation algorithm is applied twice. The first path allows the separation of the pores from the solid phase. Applied a second time, this segmentation process allows isolating the fillers from the other components [41], as illustrated in Figure 6.

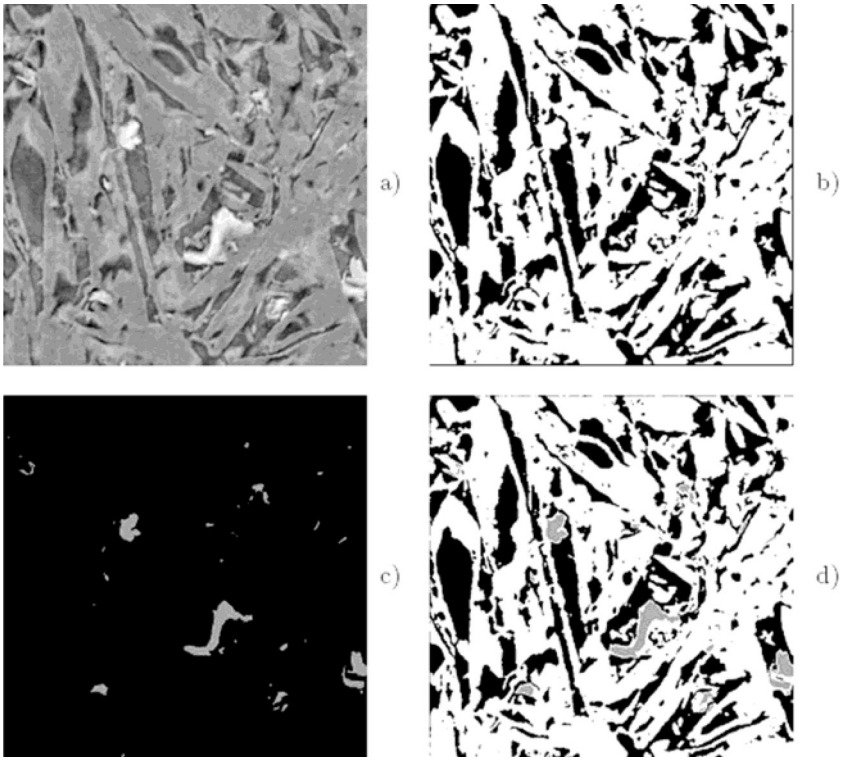

Figure 6. Different steps of the segmentation process: a) is the original slice (302 μm × 302 μm), b) corresponds to the first step (separation of pore phase), c) illustrate the separation of fillers. The last step d) is the superposition of the two previous steps.

The following images illustrate the ability to obtain a 3D visualisation and localisation of the fillers.

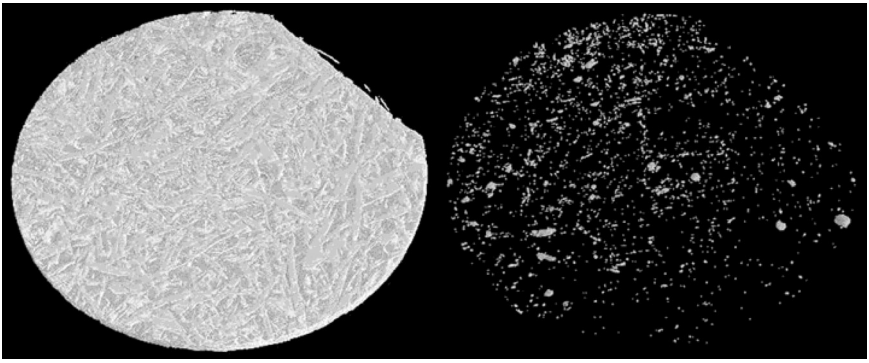

Figure 7. 3D views (1.4 mm × 1.4 mm × 150 μm) of a softwood handsheet containing about 5% of PCC: a) the three phases are presented (pores, fibres and fillers) and b) represents the spatial localisation of the fillers.

Conclusion on image processing

The separation step was briefly summarised here as several presentations and articles already mentioned the problem and their solutions in the case of paper. It must be noticed that this is the crucial point for the quantification which obviously depends on the segmentation accuracy.

Structural and topological parameters

Levitz [16] has mainly contributed to the geometrical and topological study of materials. He presented different levels of analysis:

First level: a few numbers which characterize the global properties of the porous media (porosity),
Second level: parameters such as the specific area,
Third level: The topological analysis which is related to the long range connectivity (or percolation) of the considered network.

Preliminary definitions

For each slice, a parallel beam of lines, which forms an angle θ with the abscissa, is considered to compute the following quantities:

- L_θ is the mean intercept number per unit of length, in the direction θ, between the beam and one interface.

- g_θ is the mean length on the whole space in the porous phase in the direction θ.

Let <L> and <g> be the average of these magnitudes evaluated for different angular positions.

Four variables are defined [16], namely, the porosity and the specific surface, then the integral of mean curvature and finally the integral of Gaussian curvature. As a surface may be described by two principal radii of curvature, R_1 and R_2 ($R_2 > R_1$), then the mean curvature is equal to $(1/2).(1/R_1 + 1/R_2)$ and the Gaussian curvature is $(1/R_1 - 1/R_2)$. These quantities are essential, for example, when considering the estimation of the mechanical properties. However, as the mechanical properties are not at issue here, the curvatures will not be considered further. The chord distribution is also an interesting tool (see the references included in [16]). A chord consists in a segment belonging either to the pore network or the solid phase, and having its two extremities on the interface. The two first Minkowski invariants, namely the porosity and the specific surface (ε and S_v) may be defined tracing random chords: ($\varepsilon = <g_p> / (<g_p> + <g_s>)$ and ($S_v = (4.\varepsilon / <g_p>)$, where $<g_p>$ and $<g_m>$ represent the mean chord in the pore and the solid phase, respectively. This is consistent with the definitions chosen here to evaluate such quantities.

The Saltikov relation specifies the relation between the specific surface area and the mean intercept number in all the directions of the space <L> by $S_v = 2 \times <L>$. The Tomkieff relation relates the dependency of the specific surface area, the porosity and the mean length in the pore phase <g>: $<g> = 4. \varepsilon / S_v$

Structural parameters

First level: porosity

The porosity ε is defined as the ratio of the volume of voids to the studied volume. Therefore it can be simply evaluated on digital data as the ratio of the number of voxels belonging to the pore phase to the total number of voxels.

It is obvious to understand that the porosity cannot be sufficient to characterize the physical properties of a porous media. Considering Figure 8, we plot the mixture of a highly conducting media (grey) relative to the white one. Both media have the same porosity, and the same microstructure but not the same macroscopic property.

Table 2 presents the evaluation of the porosities for the four 'reference

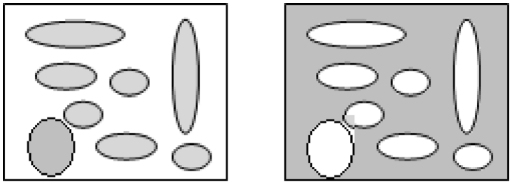

Figure 8. Schematic view of two media having the same mixture constituted of two phases: the highly conductive phase (grey) is connected only in the second structure. These structures do not have the same physical macroscopic properties.

Table 2. Porosities of the four reference samples evaluated by standard tools (ε_{meas}) and microtomographic data (ε_{tot}) [47].

	Hard	*blot*	*deco*	*Copy*
ε_{meas}	0.60	0.66	0.43	0.59
ε_{tot}	0.57	0.71	0.49	0.60

papers' presented earlier, using either the standard method or the calculation from the tomographic data.

From the preceding data, we may consider that the porosity is correctly evaluated from 3D images.

Second level: specific surface area and hydraulic radius

The specific surface area (S_v) is defined as the ratio between the wet surface and the total volume. This is traditionally evaluated on binarized data using stereology measurements [51]. Stereological tools are used to obtain information on 3D morphological properties of the studied material from 2D measurements.

We may introduce the idea to study the influence of the surface irregularity by the ratio (BS-BS')/BS where BS and BS' are the surface area before and after a smoothing procedure [7]. This comparison was checked for paper [41] proving the robustness of the method based on stereology. Unfortunately, the methods based on the direct measurement of the surface to evaluate the specific surface are very sensitive to the chosen discretisation method.

Third level: connectivity

In order to study the connectivity, two approaches are often used:

- Identifying the objects and then finding the contacts.
- Skeletonising the considered phase and deducing the objects from the skeleton analysis. Recall that the skeletonisation simplifies the pore (or fibre) space to networks in the form of nodes connected to paths.

We may note that the techniques may be used either for the pore or the fibrous structure characterisation. Some preliminary works have been published [27,36,43] for few years as for example by the active teams of Ramarao, Ramaswamy and their colleagues, (see also for example [35,52]). This work is based on the second approach. Identification of fibres and/or finding the skeleton of fibres, is currently a challenge in any fibrous material as presented in [53] for example. Some techniques have been tested without the expected success during PhD theses [27,43], in the sense that the developed tools seem not to be useable automatically to all samples of a same series. However these authors proposed ideas involving the first approach to analyze constituents' connectivity. Indeed, the most advanced results were achieved by Aronsson [27] and then by Axelsson [43] who managed to identify fibers in a wood fiber composite. This technique involves manual seed fiber followed by automatic local measurement of fiber orientation. The developed tools work on fibers that present lumen. The obtained results are exemplified in Figure 9.

Identification of pores is still an open problem. The 3D visualization of paper shows that there are two classes of voids: isolated volumes ('closed' pores) and interconnected void space ('open' pores). Characterizing the first one is trivial, since the pores represent discrete objects. However characterizing the second one is more challenging. Namely the opened porosity can be divided into two categories: the pores and the throat. Axelsson proposed an interesting approach to tackle this problem based on morphological tools and distance transform applied to the pore phases, as illustrated hereafter.

Despite these encouraging results on wood fiber composites, the topological approach requires development before it can be successfully applied to the analysis of paper applications and is consequently kept for the perspectives. Hence, a major step has to be reached in order to obtain a necessary automatic method and this is consequently a major aspect of the perspectives. This is all the more challenging as the paper structure is highly variable. In the following paragraphs, we will present only the structural analysis. Therefore, paper structure is mainly characterised by its porosity, ε, its specific surface area, S_v, its mean hydraulic radius, eventually its filler content,

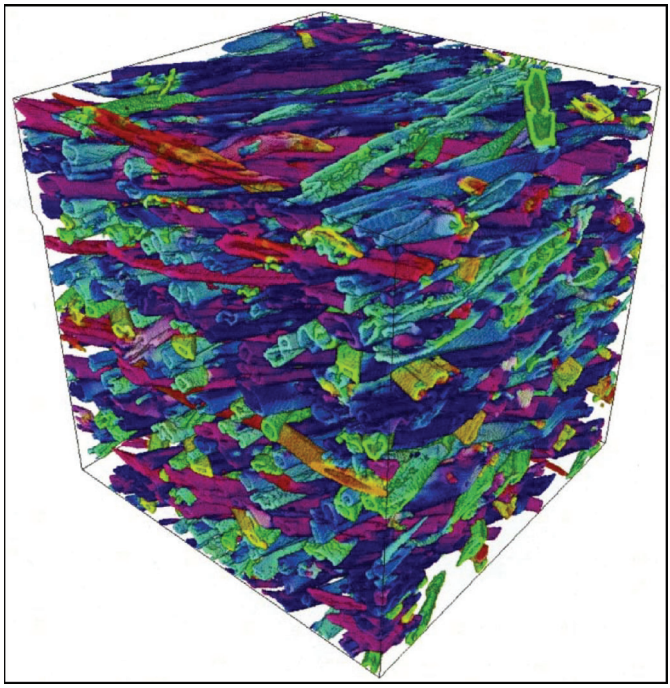

Figure 9. Volume rendering of the fibers in a wood composite material. The color corresponds to the estimated fibre orientations [43] (700 µm × 700 µm × 180 µm).

FC, and the size distribution of one of its phase. In the following paragraphs, we will present only the structural analysis.

Some 2D structural parameters

Covariance of the data sets

The structural correlation seeks to correlate the state of two distinct points separated by a distance v. It quantifies how the memory of an initial state is progressively lost when a point is moved away, as for example in a two-point correlation function.

The visualisation of the paper structure in the 3D views, suggests a strong orthotropic structure of the paper. The geometrical characterisation can be done using morphological tools ([52], [54]). In the case of a random set, the

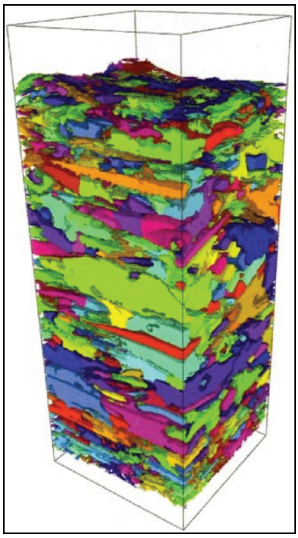

Figure 10. Volume renderings of the Individual pore based representation for a part of a cardboard sample [43] (280 µm × 280 µm × 560 µm).

covariance function is the probability for two points (s and s + v) to be in the set S where v represents a displacement vector.

$$C(S, v) = \text{Prob}\{s \in S, s + v \in S\} \tag{1}$$

The covariance has the following properties [54]:

$$C(S, 0) = V_v \tag{2}$$

and

$$\lim_{s \to \infty} C(S,s) = V_V^2 \tag{3}$$

Where V_v represents the volume fraction which is in our case the porosity. It means that the covariance function presents an asymptotic value. This value can be reached for a given $s = l_c$ that is to say before ($s \to \infty$). If it is the case, it means that the points of the structure with a distance larger than l_c are not correlated. Moreover considering different directions, the covariances give an indication of the paper structure anisotropy. In the case of stationary random set, the covariance only depends on v and is referred as C(v). In order to

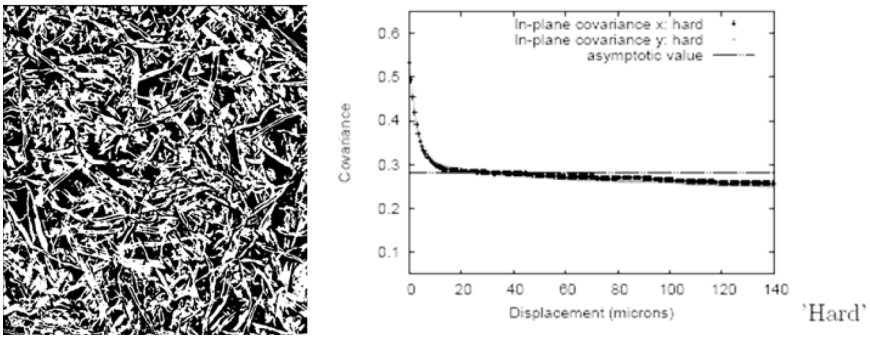

Figure 11. Microstructure of the sample 'Hard' and its covariance diagrams in the in-plane direction. In-plane slices are (700 μm × 700 μm).

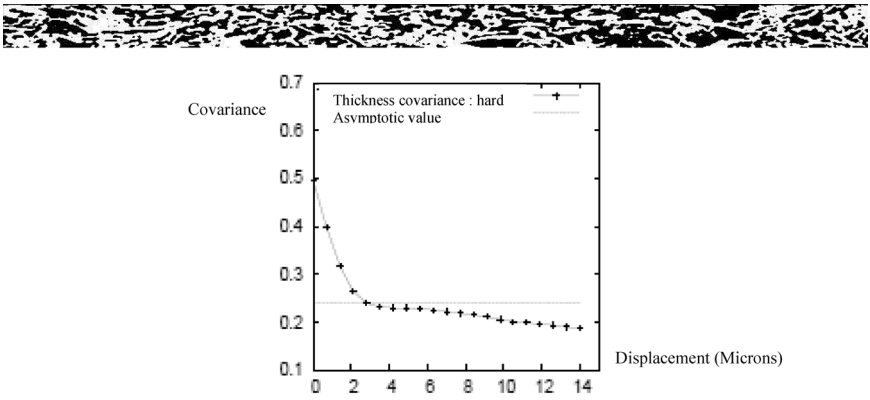

Figure 12. Microstructure of the sample 'Hard' and its covariance diagrams in the thickness direction. Out of plane dimensions are (700 μm × 35 μm).

illustrate the importance of this parameter, examples are presented. For sake of simplicity, only the 'Hard' sample will be presented.

The two above figures show the covariograms obtained in the case of a paper in the in-plane direction and in the thickness direction in the bulk, respectively. The covariograms are found equal to the porosity of the considered slice for s = 0 as mentioned earlier. The convergence of the covariance has to be studied. In the in-plane direction, they reach an asymptotic value equal to the square of porosity, for a finite range, which fits to the definitions. However, it has to be noted that the porosity, in this illustration, was

calculated in sake of simplicity on a 2D slice instead of the whole structure, as it should have been done.

They reach this asymptote for the same value (called covariance range) in both in-plane directions which confirm the isotropic in-plane structure, in comparison to the thickness direction. The covariance diagrams in the thickness direction are quite different: they do not reach an asymptotic value at the observation scale. The covariance range characterises the heterogeneity length in the studied direction.

Table 3 summarises the obtained covariance lengths for the samples described before. The anisotropy rates l_{cx} / l_{cz} confirm the strongly orthotropic structure that can be observed on the 3D views of the samples. The heterogeneity length in the in-plane direction is typically about 30 microns and in the thickness direction is about 5 microns. This kind of behaviour is similar to the one find in the literature [35].

Geometrical anisotropy

The determination of the geometrical anisotropy characterisation in the in-plane direction in the case of paper samples acquired by synchrotron X-ray microtomography is also interesting.

The geometrical anisotropy is here characterised on images by evaluating either the intercept numbers or the pores lengths for different angular positions and finding their minimum and maximum values. Anisotropy can be characterised by an ellipse and in particular by its ellipticity ([55], [56]). Namely a circle is characteristic of an isotropic structure whereas a higher ellipticity reflects a higher anisotropy. Let a, be the major axis of the ellipse and b, the minor one. The obtained value can correspond either to the intercept number or to the chord length. The rate a/b represents the ellipticity, which is used for anisotropy characterisation.

The samples analysed in this aim are five different oriented papers called 15, 16, 18, 19, and 20 which have been previously described by Silvy [56]. The

Table 3. Covariance range of the four reference samples. l_{cx} represents the in-plane covariance range, l_{cz} the thickness one and l_{cx} / l_{cz} characterises the microstructural anisotropy rate.

Sample	*Hard*	*Blot*	*Deco*	*Copy*
l_{cx} (µm)	33	26	31	20
l_{cz} (µm)	2.5	3.5	5.5	4.5
l_{cx} / l_{cz}	12.4	7.4	5.6	4.4

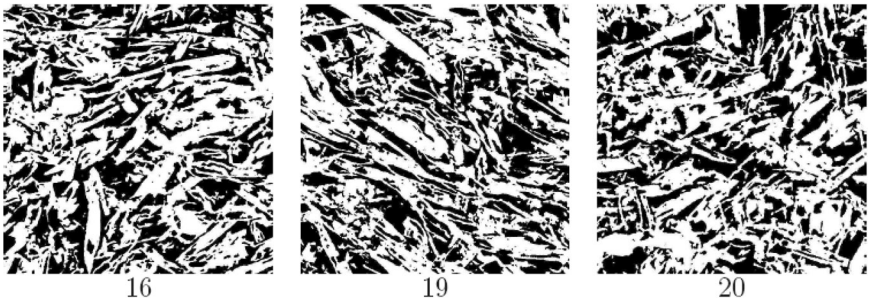

Figure 13. In-plane slices of three oriented papers (490 μm × 490 μm).

different fibre orientations were obtained on an industrial machine. Three of them are presented in Figure 13. They are made of bleached softwood fibres beaten to 25 °SR.

On these pictures, we can observe the isotropic structure of the sample 20 where no preferential orientation appears. The samples 16 and 19 present anisotropic structure in term of fibre orientation. These papers have been previously characterised using other experimental tools, as for example in [57]. Table 4 presents the ellipticities evaluated on microtomographic data and the ones presented in different studies ([56], [57], [58]) for the five samples.

This table indicates that the covariance lengths in the main in-plane directions can also be used as an indicator of the geometrical anisotropy. It should be noticed that the two means used to characterise the geometrical anisotropy do depend on the considered methods. Nevertheless it should be noticed that the classification obtained on tomographic data is the same as that obtained with the other techniques. Bloch [57] demonstrated that each anisotropic measurement technique gives its own magnitude but preserves the relative order between the samples. Consequently, we may consider that the evaluation of geometrical anisotropy on microtomographic data can be carried out [33]. Holmstad and his co-author carried out a similar work based on the

Table 4. Comparison of the geometrical anisotropy obtained on tomographic data and with classical tools for the five oriented samples.

Sample	*18*	*19*	*20*	*16*	*15*
l_{cx}/l_{cy}	1.5	1.64	1.1	1.3	2.9
a/b tomo	1.23	1.13	1.09	1.16	1.21
a/b literature	2.6	1.7	1.4	1.7	2.2

previous theoretical works of Silvy ([59], [60], [55,61,58]) but they found higher values than the experimental values obtained with classical tools. They suggested that it may due to the small volume imaged which could be the case as their imaged volumes (500 µm × 200 µm × paper thickness) are generally smaller than the estimated in-plane REV.

Some 3D structural parameters

Porosity profiles

The porosity profiles in the thickness direction of these four reference samples are presented in Figure 14.

For a better comparison between the samples, the thickness is reported as a function of (z/h) where z and h represent its coordinate and its thickness, respectively. These porosity profiles are similar to the ones presented on fibreboard materials using a confocal microscope [26]: a decrease in porosity at the top surface, a plateau and finally an increase in porosity. The plateau corresponds to the bulk whereas the two strong porosity gradients correspond to the outer layers. Such porosity profile is due to the paper making process. We

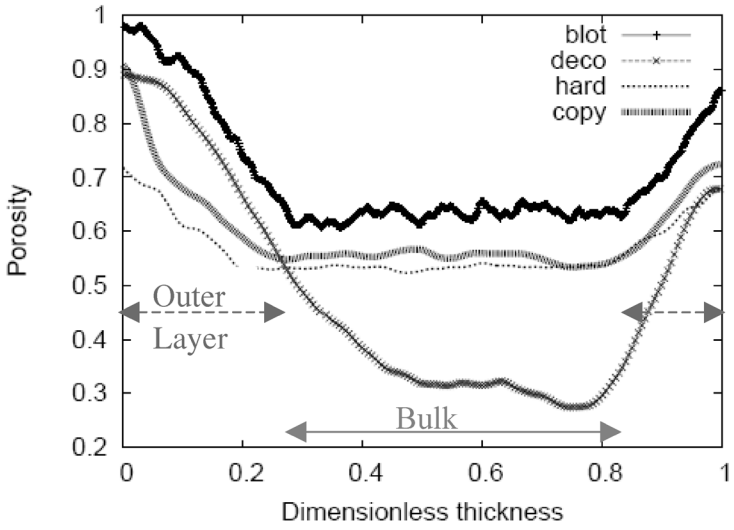

Figure 14. Porosity profiles in the thickness direction of the four reference samples: 'hard', 'blot', 'deco' and 'copy'. To directly compare the profiles, the thickness is reported in its dimensionless form. The dotted arrows and the continuous feature represent the outer layers and the bulk, respectively.

found that the thickness of these outer layers is equal to about 50% of the total thickness. It is clear that these outer layers play a crucial role in the end-use properties such as printability, for example. Moreover, this variation of porosity in the thickness direction has some influence on the mechanical behaviour as proved for other materials such as composite [62]. Moreover, Dodson [63] introduced in this conference, the pore in the bulk and the surface pores in layered random fibre network. However, the distributions of these two classes of void height were indistinguishable in his results. Nevertheless, this is well known is the context of the papermaking and cannot be ignored neither in the theoretical nor in the modelling developments.

Table 5 represents the obtained results concerning porosity on the whole sample ε_{total} and on the bulk ε_{bulk} (1000 µm × 1000 µm × bulk thickness µm) evaluated on microtomographies for the four samples and with classical tools $\varepsilon_{measured}$

Table 5. Porosity of the four reference samples evaluated by classical tools (ε_{meas}) and microtomographic data either for the whole sample (ε_{tot}) or only in the bulk (ε_{bulk}) [47].

	hard	*blot*	*deco*	*Copy*
ε_{meas}	0.60	0.66	0.43	0.59
ε_{tot}	0.57	0.71	0.49	0.60
ε_{bulk}	0.53	0.64	0.31	0.54

We may observe differences between the total porosity and its value calculated for the bulk.

Surface specific profile

We obtain similarly the profiles of the specific surface, presented in Figure 15.

The profile of the specific surface is consistent with the evolution of both the porosity and the hydraulic diameter.

Filler content

The filler content (FC) is classically evaluated by destructive method [ISO 2144, 62]. This consists in weighing the sample before and after burning it at a temperature of 800°C +/– 25°C. The ash rate is evaluated here as follows: $FC = m_c / (m_c + m_f)$, which becomes: $FC = N_c.d_c / (N_c.d_c + N_f .d_f)$ for numerical data where m, N and d represent respectively the mass, the number of voxels and the density. The subscripts c and f represent the fillers and the

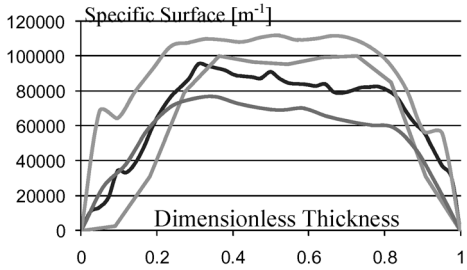

Figure 15. Profile of specific surface Vs. Dimensionless Thickness (Up to down, samples: Hard, Copy, Blot and Deco).

fibres, respectively. Table 6 presents the characteristics of some classical fillers, the fibre density being 1540 kg.m^{-3}.

Figure 16 represents the visualisation of hand sheets containing fillers. The left images represent the grey levels of a slice extracted from a 3D volume obtained using microtomography. The images on the right show the slice after segmentation.

We may remark the ring artefact on the first image. Few tools exist nowadays to eliminate such rings as for examples the one developed in [43]. Furthermore, the shape of the fillers may be studied as for example the method developed by Lin [64].

In order to validate quantitatively the amount of fillers, some handsheets were realised using Eucalyptus and various fillers with different amounts of them. Their filler contents evaluated either considering the standard or the microtomographic data (for both the bulk and the total structure). The results [41] are presented in Table 7.

We may therefore conclude that the proposed method is validated. We may also note that it is not efficient for the clay due to its physical composition, such that its X-ray attenuation is close to that of the cellulosic fibers. However, the preceding results prove that these analyses of the microtomographic images are consistent with the standard measurements. The next step is to

Table 6. Characteristics of the studied fillers: density and specific surface area. These values were found in mineral index data bases.

Filler	*GCC or PCC*	*Ti02*	*talcum*	*clay*
Density (kg.m^{-3})	2900	4000	2750	1700
Specific surface area S_v (m^2.g^{-1})	3–9	9	10–16	15–30

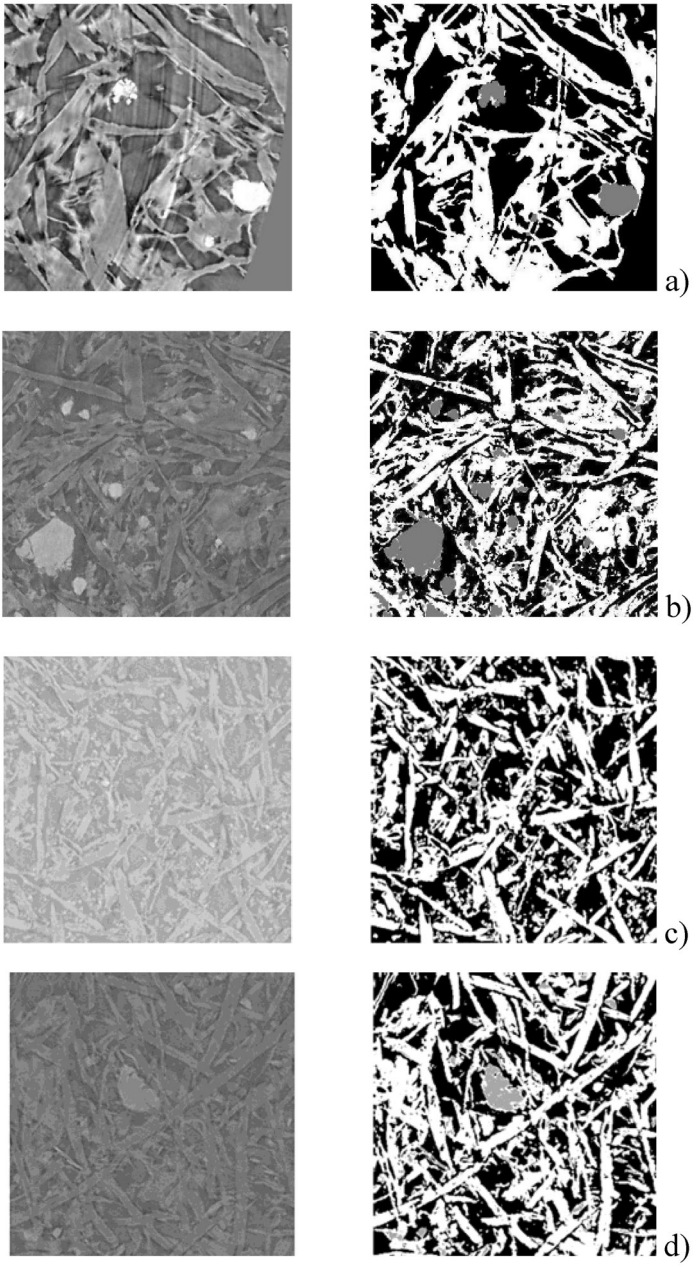

Figure 16. Segmentation of the handsheets filled with different fillers. The slices are 358 μm × 358 μm. The left slices correspond to the original data whereas the right ones represent the corresponding segmented slice: a) Softwood handsheet in which about 5% of GCC is added, b) Eucalyptus handsheet that contains 18.4% of Ti02, c) Eucalyptus handsheet that contains 6% of PCC and d) Eucalyptus handsheet that contains 9.1% of talcum.

Table 7. Filler content evaluation for series of handsheets.

Fillers	*Standard rate (%)*	*Content Total (%)*	*Content Bulk (%)*
TiO_2	18.4	19.5	18.0
TiO_2	18.4	17.9	15.5
TiO_2	8.2	8.9	9.7
TiO_2	8.2	8.9	8.5
PCC	9.8	11.4	13.7
PCC	6.0	6.9	6.1
Clay	14.5	2.3	/
Clay	8.8	1.3	/
Talcum	13.8	13.5	14.2
Talcum	9.1	8.9	7.1
GCC	10.2	12.4	14
GCC	3.4	4.4	4.3

check the validity of these preliminary conclusions, that is to say answer the following question: are the volumes big enough to validate the quantitative measurements? This question is raised in the following paragraph.

REPRESENTATIVE ELEMENTARY VOLUME (REV)

Introduction

Most of the studies ([[50], [48], [25], [65], [35]) on paper structure characterisation by X-ray synchrotron radiation microtomography relate numerical results concerning the structural properties or the physical characteristics. They are based on the assumption of the existence of a Representative Elementary Volume (REV).

However no characteristics length (l_{REV}) was reported. This length should satisfy the separation scale needed for homogenisation theory. We typically should have:

$$l_{micro} << l_{REV} << l_{macro}$$

Where l_{micro} and l_{macro} represent respectively the micro scale and macro scale.

The REV can be defined as the smallest volume that represents the sample for a given physical property and for a given error. This study on the

representativity of samples imaged by synchrotron XRM has been successfully carried out on different materials such as sandstone [66], metallic alloy [67] or composites [68]. As the volume imaged in the case of paper (1.4 mm × 1.4 mm × paper thickness) is much smaller than the typical size of a paper sheet, the volume imaged has to be proved to be sufficiently large to allow the quantification of structural parameters such as porosity, specific surface area or filler content.

The numerical technique to evaluate structural parameters on segmented data is presented here. As the previous works showed it, the structural values obtained on data from microtomography have the same order of magnitude as the one obtained with classical tools. Two sets of samples are reported. The first one is dedicated to the porosity and specific surface area studies and the second one to the filler content. Finally, the evaluation of the REV is carried out. Different techniques ('deterministic' and 'statistical' approaches) to evaluate may be applied for the structural analysis (porosity, specific surface area and filler content). They will be described and compared.

Definitions

Different definitions can be found in the literature to characterise the Representative Elementary Volume (REV). Stroeven and Kanit proposed overviews of them ([69], [70]):

- Hill [71]: The REV should be large enough to contain sufficient information about the microstructure in order to be representative. This volume is supposed to be large enough to be statistically representative of the sample that is to say it contains enough heterogeneities.
- Drugan [72]: The REV is the smallest volume that still represents the materials for a given property. It gives smaller REV than the one obtained with the previous method but does not take into account the statistical fluctuations.
- Gusev [73]: The minimum REV is evaluated for a given property on a finite number of realisations. The obtained average must be constant and the scatter should be small.

It has to be noted that the REV is associated to a physical property, a structure and a relative error. In such a context, the REV length, l_{REV}, can be defined as a number of heterogeneities so called 'deterministic' approach ([74], [47]). Kanit and his co-authors [75] suggested estimating it as a function of the number of realisations for a given relative error. The realisations can be defined either as different analysed samples or as different non-overlapping

sub-volumes extracted from a single sample. This is referred as the 'statistical' approach.

Both methods are applied and compared in the following sections.

Evaluation of the 'deterministic' REV

As proposed by Drugan [72], the REV can be estimated in a 'deterministic' way by evaluating the property of interest for larger and larger volumes always centred on the same voxels. This 'deterministic' REV size is given by the size of the volume for which the fluctuations of the studied property become limited.

The microstructural properties are evaluated for samples of volume ($l \times l \times 35$ μm) where l represents the side length and varies from 50 μm to 700 μm. The Figure 17 represents the evolution of the porosity as a function of the length l for a given thickness of 35 microns for the four reference samples.

We also investigate in the same way the filler content by representing the evolution of filler content as a function of length l. The results are presented hereafter.

These graphs indicate that the studied properties namely porosity and filler content, reach an asymptotic value for a length of about 400 μm. Moreover the eventual presence of fillers ('deco' and 'copy') does not affect the size of

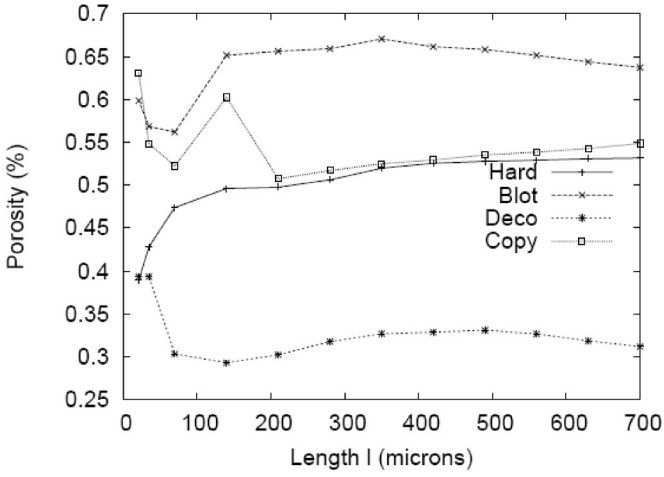

Figure 17. Evolution of porosity as a function of the length l for a given thickness of 35 microns for the four reference samples ('hard', 'blot, 'deco', 'copy').

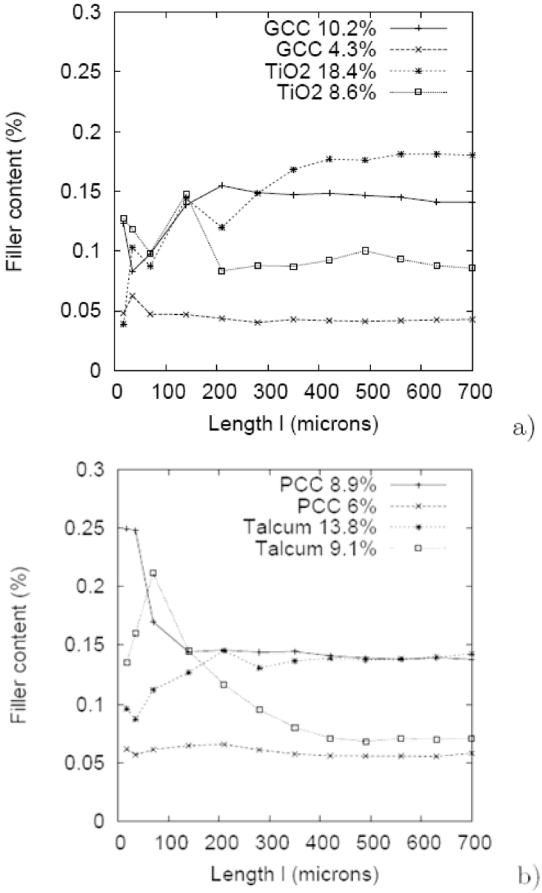

Figure 18. Evolution of the filler content as a function of the length *l* for a given thickness of 35 microns for different filler contents and various kinds of fillers.

the stabilisation length for porosity. It is neither affected by the filler sizes nor the filler content.

These evolution graphs are typical of the existence of a REV as presented in [72]. Its size may be quantitatively estimated. As mentioned earlier, a REV is always defined by a set of characteristics: a sample, a property and a relative error. The typical size of a REV, l_{REV}, can be defined as a given number (N_h) of heterogeneity lengths as proposed by Ostoja-Starzewski [74] or Rolland du Roscoat [41]. The heterogeneity length chosen here is the

covariance length obtained in the previous section. The l_{REV} can be expressed as follows: $l_{REV} = N_h \times l_{cx}$.

The next step consists in the evaluation of the relative error made for a given number of heterogeneity lengths. The reference values are the values obtained on the bulk of the samples. Let ε be the studied property, ε_l the evaluation of this porosity for a bulk of size ($l \times l \times 35$ µm) and ε_{bulk} the value obtained on bulk of size (1000 µm × 1000 µm × 35µm). The relative error is therefore: $err = (\varepsilon_{bulk} - \varepsilon_l)/\varepsilon_{bulk}$.

The values of ε_{bulk} are reported in previous tables for micro structural properties and filler content, respectively. The relative error obtained for each sample is reported in Table 8 for $N_h = 10$ and $N_h = 20$, for structural properties.

Table 8 indicates that these samples are representative from a micro structural point of view concerning the 'deterministic' REV. As expected, if the number of heterogeneity lengths N_h increases, and thus the size on which the property is evaluated, the relative error made on its estimation decreases.

Evaluation of the 'statistical' REV

This part is dedicated to the influence of fluctuations on the REV by considering as an illustration a given thickness of 35 µm. In order to determine the 'statistical' REV size for the micro structural properties, the porosity and the dimensionless specific surface area are evaluated for 5 different sub volumes (V_i) that do not overlap and that are arbitrary chosen in the sample. The length of these sub volumes varies within the range 21 µm to 280 µm. V_1 corresponds to the volume presented in the previous section. The Figure 19 shows the evolution of the mean porosity as a function of the length *l*. We also indicate the 5 different values obtained at a given length *l*. This is done for the four reference samples.

These curves show that the porosity of a given sub-volume stabilises and reaches the reference values presented in previous tables. When the side

Table 8. Evaluation of the relative error [%] made on the estimation of the porosity for a given number Nh of l_{cx} at a given thickness of 35 µm.

Sample	*Structural Property*	*Hard*	*Blot*	*Deco*	*Copy*
$l_{REV} = 10 \times l_{cx}$	Porosity ε	3.5	4.3	5.0	11.6
$l_{REV} = 20 \times l_{cx}$	Porosity ε	0.3	3.1	2.3	5.6

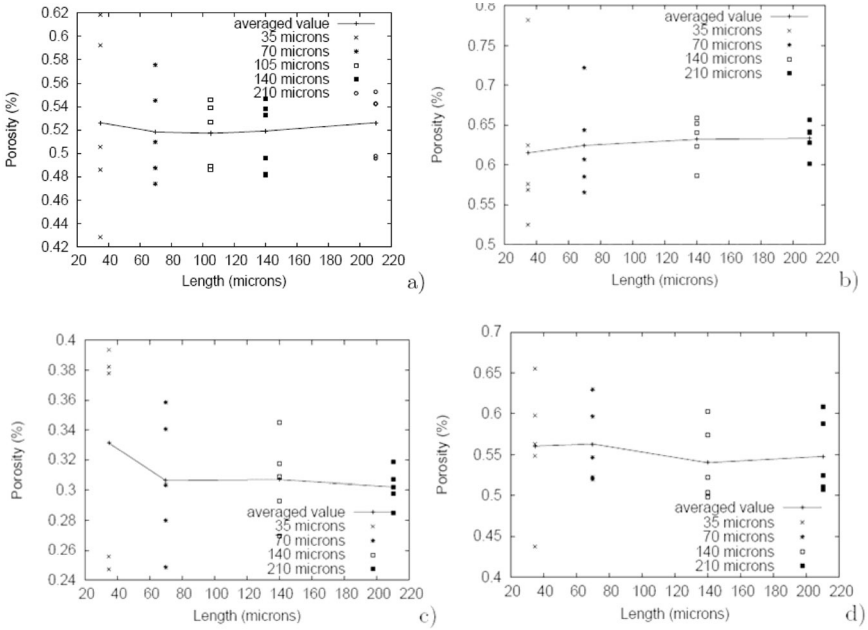

Figure 19. Evolution of the porosity for the four reference samples that are a: 'hard', b: 'blot', c: 'deco', d: 'copy'. The dots represent the values obtained for the five non overlapping sub-volumes of side length *l*. The continuous line corresponds to the average for a given length *l*.

length increases, the dispersion of the results decreases, as expected. Averaging these values [73], the mean of the micro structural properties converge to the final value for a length *l* of about 100 μm. These tendencies are similar to those already observed for the micro structural properties of sandstone [76] and for effective physical properties such as in the works of Kanit [69]. This suggests that the micro structural properties can be deduced from volumes smaller than the REV provided that there are a sufficient number of realisations [75].

Kanit and his co-authors define the 'statistical' REV size as a function of the physical properties of each constituent, their microstructure, the required precision and the number of realisations. This 'statistical' REV size is based on the notion of integral range A3 which depends on the studied property. This range gives information on the domain sizes needed to have a good statistical representativity [54] or the seminal works of Matheron in 1967 [52].

The integral range A_3 is linked to the scatter in apparent properties $D_{Ap}(V)$ found on sub volumes of fixed size V and containing several realisations N of the microstructure:

$$D_{Ap}^2(V) = D_{Ap}^2 . \frac{A_3}{V} \tag{4}$$

Where D_{Ap} represents the point variance of the apparent property studied.

These authors also show that the smallest volume V (N, err, Ap), necessary and sufficient, to estimate the studied property with a given relative error, err, and number N of realisations are linked by the following relationship:

$$V(N, err, Ap) = \frac{4}{Ap^2} . \frac{D_{ap}^2}{err^2} . \frac{A_3}{N} \tag{5}$$

We detail these relations first for the case of porosity as presented in Kanit ([69], [75]):

$$D_\varepsilon^2 = \varepsilon . (1 - \varepsilon) \tag{6}$$

Introducing these two equations into the definition of $D_\varepsilon(V)$, leads to the following expression dedicated to porosity:

$$D_\varepsilon^2(V) = \varepsilon_{bulk} . (1 - \varepsilon_{bulk}) \frac{A_3}{V} \tag{7}$$

Where D_ε^2 represents the variance of the porosity evaluated for the sub volumes of size V.

Kanit and his co-authors also showed that the smallest volume V (N, err, Ap), necessary and sufficient, to estimate the porosity with a given relative error, err, and number of realisations, N, are linked by the following relationship in the case of porosity:

$$V(N, err, \varepsilon) = \frac{4(1 - \varepsilon_{bulk})}{\varepsilon_{bulk}} \frac{A_3}{N . err^2} \tag{8}$$

We may note that considering the case of the specific surface area, Jeulin [77] evaluated the point variance of the specific surface area for an anisotropic structure.

Table 9 presents the obtained results for the porosity. The integral ranges

Table 9. Results of statistical l_{REV}, evaluation of A_3 and number of correlation lengths to reach the final bulk value with a given error, err, with N realisations in the case of porosity.

Sample	A_3 (μm^3)	*Err (%)*	*l (err, N=1)* (μm)	*l (err, N=5)* (μm^3)
Hard	800	3.6	250 ~ 8 × l_{cx}	111 ~ 3.6 × l_{cx}
Blot	1600	4.3	241 ~ 9.2 × l_{cx}	61 ~ 4.1 × l_{cx}
Deco	1000	5.0	318 ~ 9.6 × l_{cx}	142 ~ 4.3 × l_{cx}
Copy	540	11.6	61 ~ 3 × l_{cx}	27 ~ 1.3 × l_{cx}

are reported and the size of the REV for a given error and two given numbers of realisations. Here the error is the relative error between the property estimated on the whole bulk (1000 μm × 1000 μm × bulk-thickness) and on the studied bulk (700 μm × 700 μm × 35 μm).

The results in Table 9 indicate that the REV for microstructural properties can be evaluated using statistic tools on sub-volumes smaller than the 'deterministic' REV provided the number of realisations is sufficient.

Conclusion

In this section, the representativity of the samples described in previous sections for the different microstructural properties is investigated. Before introducing the necessary definitions, we would like to mention the work of Hazlett [78], and the references included. The idea was to study the influence of the variability on the structure through simulated images of porous structures. Sub-images were extracted from the main one. Here, the important conclusion is that working on simulated image, the correlation length has to be introduced, but also the variation of the structure, in particular if the connectivity or the permeability is considered. He insists on the presentation, of the mean values, the error bars and the coefficient of variation in each direction. It is also interesting to cite a previous sentence extracted from a previous article of the same author [79]: '*The need to generate artificial media is lessened by the availability of micro-imaging technique*'. However, as presented before, we do not agree with such a sentence, estimating that there should be complementary approaches.

It appears that the imaged volume was larger than the REV. Therefore structural characterisation and quantitative measurements may be carried out. This characterisation concerned here the geometrical anisotropy, the

granulometry of the considered phase and the filler content study. However, the influence of higher length scale (formation) was not on the scope of this work, as another range of characteristic length had to be introduced. The presented work validated *a posteriori* the published works on microtomography of other authors as we had proved that the REV was usually smaller than the image analysed. Consequently, the quantitative data extracted from the measurement may be considered as correct.

EXPERIMENTAL RESULTS AND COMPARISON TO THEORIES

It is important here to underline again that there exist clear complementarities between the development of experimental tools that allow characterising the porous structure of papers and the requirement for associated theories. Indeed, some measurements may be carried out on papers, in order to study either the raw materials or any unit operation, such as beating or pressing. However, it is almost impossible to study experimentally the influence of a single parameter on the fibrous structure. Indeed, several fibre morphological properties are modified simultaneously during an industrial operation. That is the gap where the models are necessary. We do not want to introduce here the simulation of physical properties, as it is not on the scope of this paper. Some presentations in this conference were dedicated to this, such as the one presented by Koivu and *et al.* (2009) dedicated to *flow permeability of fibrous material. Microtomography and numerical simulations*. Furthermore, some interesting works dedicated to this aspect are numerous, as for example [80,81] or [82].

Concerning the theoretical development, we would like to underline the work carried out at Manchester [3]. The idea is here only to briefly illustrate the approach, namely to compared the experimental parameters and their evolution to existing theories. The first part will consist in the important concept of Relative Bond Area (RBA) and the second one will deal with the structure characterisation.

Relative Bond Area

It is important also to note that both fibrous and porous phases may be characterised in the image analysis, that is to say either the fibrous or the porous structures. Classically, the fibres are characterised before the structure is elaborated and also in their final state in paper. Some characteristics are essential, such as for example the number of contacts per volume or the Relative Bond Area (RBA). We present here this concept as it represents

the next important characterisation to be determined in order to reach new perspectives in both the characterisation and the numerical simulation, in particular, if the mechanical properties are studied. We will review the main contributions since 1959.

One possible starting point may be the work of Ingmanson [83]. He presented the two classical experimental methods that is to say the optical and the adsorption ones. Furthermore, it is interesting to remind the definition of the RBA, as two approaches may exist considering either the bonded or the unbounded surface areas:

$$\frac{A_B}{A_T} = \frac{A_T - A_{UB}}{A_T} \tag{9}$$

Where A_T, A_B and A_{UB} represent the total available surface area for fibre bonding, the bonded and unbounded areas, respectively.

Therefore two approaches exist either the direct (determination of the external bonded area of the fibres) or indirect ones (determination of the unbonded area of the fibres). A useful concept may also be introduced here: the bond density, which is defined as the number of bonds per unit bonded area.

The discussion on the optical method consists essentially on the relation between the coefficient of diffusion S deduced from the theory of Kubelka-Munk, and the specific surface of the material, evolving for example due to the fibrillation that may occur during beating.

We would like to cite Ingmanson, as his contribution will be discussed in the next contributions: '*At the same total bonded area, the tensile strengths of the pulps are the same irrespective of degree of refining, the amount of fines, or the extent of wet pressing*'. Figure 20 illustrates his results.

In another work [84] of the same period, the obtained experimental results '*indicate that bond density (bonding strength per unit area) increases with the degree of beating*'. They also claimed as the initial results presented by Hazelton ([85,86]) concerning the '*excellent correlation between the specific scattering coefficient of unbleached sulphite handsheets and the area obtained by adsorption of nitrogen*'. However Luner and *et al.* [87], claimed that the scattering method is not correct in contradiction to the work of Haselton. He proposed instead to plot the coefficient S versus the Young Modulus and to compare a series of pulps at the same extent of refining. Kallmes [88] insisted on the problem of the uncollapsed part of the lumen for both measurement techniques. He also introduced the important idea that the main morphological property for the RBA, consists in the fibre width. However, the

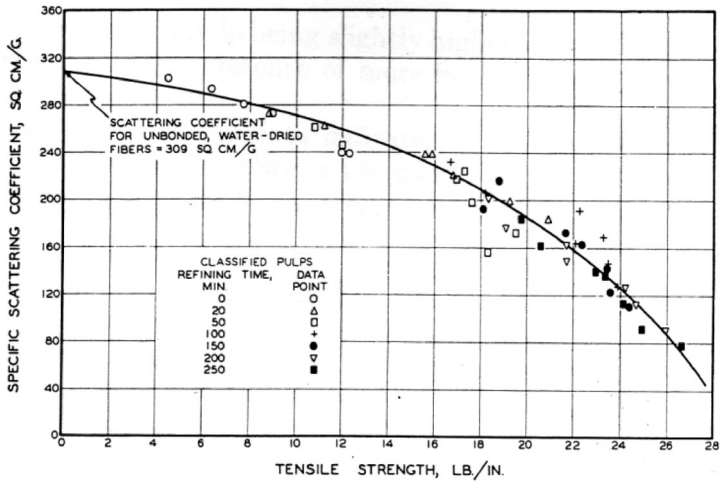

Figure 20. Scattering coefficient – tensile strength relationship at various wet-pressing and refining intervals for classified pulps [83].

proposed method based on visualisation using a microscope has been criticised afterwards. However, the following illustrations are interesting.

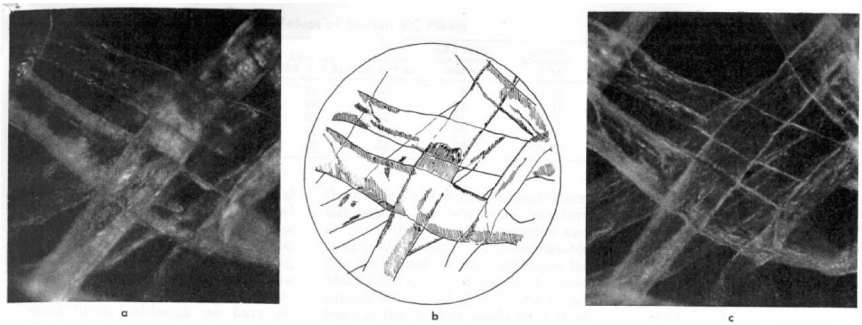

Figure 21. Same view shown under reflected, polarized light (a), and dark field illumination (c). Collapsed and uncollapsed parts of the fibers shown cross-hatched in (b), pictorial of fibers in micrograph; cross-hatched parts of fibers represent areas not in optical contact [88].

He also presented a clear visualization of the contact analysis in the following picture.

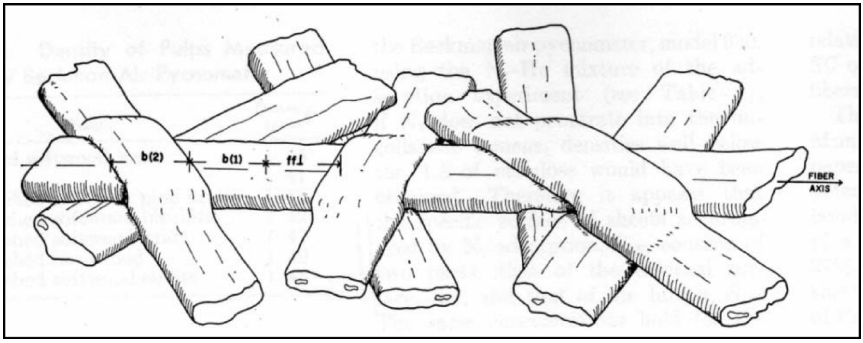

Figure 22. Structural component of paper [88]. Visualization of the free fiber length, the lengths bonded on either one or both sides. The bonded area may be defined from these quantities.

Skowronski [89] introduced an interesting experimental approach to estimate the breaking energy of fibre-fibre bond which will be the next step in the perspectives concerning the simulation of 3D structure. That may also constitute a useful technique to validate the numerical simulation.

Concerning the more recent theoretical approach, Soszynski [90] proposed a theoretical equation to estimate the RBA based on the numbers of layers of fibres and the probability of finding a fibre. The major contributions have been proposed by Batchelor on one hand and Sampson on the other. Batchelor [91] proposed to introduce the cross-sectional shape of fibre. Moreover, he proposed an interesting method that aims to measure the bonding in machine-made papers. Later, he also developed an analytical model to establish the number of fibre-fibre contacts and expressions for RBA [92]. Sampson proposed the most advanced theoretical model for fibre contact in planar random fibre network [93] and more recently in [3]. He introduced different quantities such as the number of crossing per fibre, the distance between such crossings, in order to evaluate the expected pore area. Furthermore, he proposed an estimation of the area of a single crossing and the number of crossing per fibre. Batchelor and Sampson [94] have published a 2D comparison between theoretical and experimental results. Clearly, the perspective to characterise these quantities directly on measured 3D structure of paper at the fibre scale, will complete this approach. This will constitute a major objective of the analysis of the 3D structure.

Structure characterisation

The modelling investigations concern the characterisation of the pore size distribution from a global point of view. The developed models were until recently applied to experimental data obtained in an invasive way (flow or mercury porometer) or with destructive techniques (microtome images). Therefore, we compare here the structural results obtained on the 3D segmented microtomographic data of paper and the theoretical model or experimental results. The first one refers to the modelling of the pore height distribution in the thickness direction. The second comparison concerns the influence of the paper making units on the pore size distribution. The study concerning these two points is developed as follows: the model and experimental results found in the literature are summarised, the samples of interest are described, the structural results obtained on these samples are presented and finally compared to the models. We may remind that in the previous chapter, we demonstrated that a volume of (700 μm × 700 μm × 35 μm) extracted from the bulk is larger than the representative volume and that quantitative measurements can be carried out on such volume.

Out of plane pore size distribution

In this section, attention is focussed on the pore height (h) and its distribution in the paper thickness direction. This study is carried out on the four reference samples described in the previous chapter in order to illustrate the demarche and the potential of this 3D analysis.

Different models are proposed in the literature to fit the distribution of pore height h in the thickness direction. Niskanen [28] suggested using the following distribution:

$$f_1(h) = (1-q).q^{\frac{h}{a-1}} \tag{10}$$

Where a represents the pixel size and q can be related to the porosity ε and to the fibre thickness t by the proposed following relation:

$$q = \left(1 + \frac{1-\varepsilon}{\varepsilon}.\frac{a}{t}\right) \tag{11}$$

The mean $\mathbf{h}_1$ of such a distribution ($f_1(h)$) equals:

$$\mathbf{h}_1 = \frac{a}{1-q}. \tag{12}$$

and its standard deviation std1(h):

$$\mathrm{std}_1(\mathrm{h}) = \frac{\sqrt{\mathrm{q}}.\mathrm{a}}{1-\mathrm{q}} \tag{13}$$

Recently, Urquhart suggested using a negative exponential distribution [95]

$$\mathrm{f}_2(\mathrm{h}) = \frac{\exp(-\mathrm{h}/\mathbf{h})}{\mathbf{h}} \tag{14}$$

Where **h** represents the mean.

Its mean is equal to:

$$\mathbf{h}_2 = \frac{1}{\mathbf{h}} \tag{15}$$

and its standard deviation:

$$\mathrm{std}_2(\mathrm{h}) = \frac{1}{\mathbf{h}} \tag{16}$$

Sampson also suggested applying a gamma distribution:

$$f_3(\mathrm{h}) = \frac{\mathrm{h}^{k-1}\exp(-\mathrm{h}/b)}{\Gamma(k).b^k} \tag{17}$$

Where b and k represent the parameters of this distribution.

Its mean is equal to:

$$\mathbf{h}_3 = \frac{k}{b} \tag{18}$$

and its standard deviation:

$$std_3(\mathrm{h}) = \frac{\sqrt{k}}{b} \tag{19}$$

Figure 23 presents for the four reference samples the original distribution on which the three different modelled distributions are superposed.

Table 10 summarises the parameters of these distributions for the four reference samples.

These results indicate that these data are well represented by a gamma distribution with a coefficient of determination of about 88%. Nevertheless

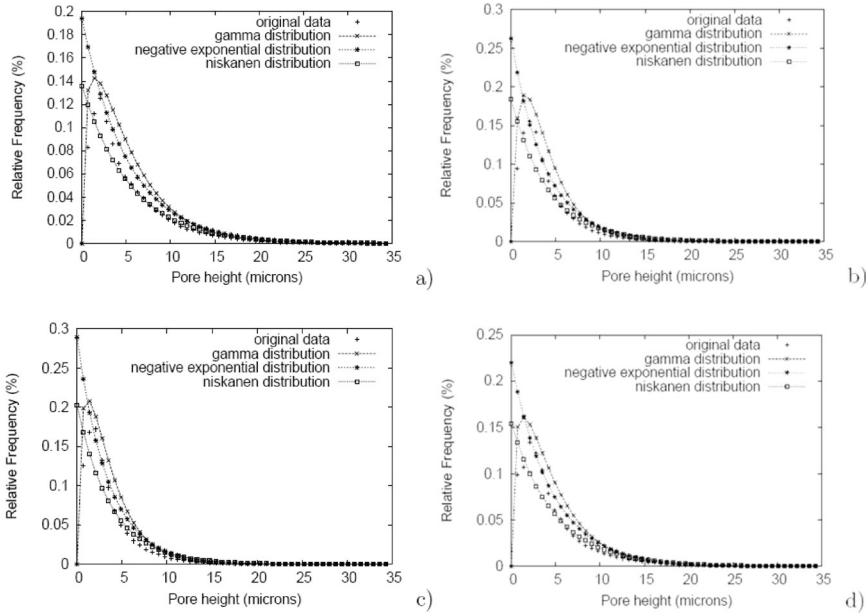

Figure 23. Distributions of the pore height in the thickness direction. Original data and the different models are plotted for the four reference samples: a) hardwood handsheet, b) blotting paper, c) decorative paper and d) printing paper.

Table 10. Parameters estimated (mean pore height **h** and standard deviation std(h) of pore height) from the original distribution and parameters deduced from the previous ones to fit the proposed distributions. h and std(h) are expressed in microns. b, k and q represent the parameters of the model.

Sample	*h*	*std (h)*	*b*	*k*	*q*
Blot	3.9	2.92	0.45	1.7	0.84
Hard	5.2	4.38	0.26	1.4	0.88
Deco	3.5	2.81	0.43	1.5	0.83
Copy	4.6	3.83	0.31	1.4	0.86

these gamma distributions are close to negative exponential distributions as k tends to 1. If we consider that the smallest pore size distribution corresponds to one voxel (0.7 μm^3), the distribution proposed by Niskanen seems to be the more adapted with a coefficient of determination greater than 90%. It fits

with the experimental resolution and neglecting the pixel size in his model. Further validations should be carried out.

Influence of paper making parameters on the pore size distribution of the paper bulk

Global models coupled with experimental results [1,96,95,97] describe the effect of unit operation unit of papermaking process (refining) and grammage on the pore radius (r) distribution. The pore size distributions are characterised by their maximum pore radius (max(r)), mean pore radius $\bar{r}$ and the standard deviation of pore radii (std(r)). Dodson and Sampson [98] presented the probability density function g(r) for the pore radii r as:

$$g(r) = \frac{4b^{2k}.\pi^{k} r^{2k-1}.K_{0}(z)}{\Gamma(k)^{2}} \tag{20}$$

Where k is a shape factor, b a scale factor, $\Gamma(k)$ refers to the gamma function, $K_0(z)$ represents the zeroth order modified Bessel function of the second order and $z = 2br\sqrt{\pi}$.

Urquhart [95] reported in his PhD, experimental results showing that the mean pore radius is independent of the grammage for unbeaten samples and decreases with increasing grammage for beaten samples. On the other hand, Dodson and *et al.* [97] found an increase of both quantities with a decrease of the grammage regardless the refining degree. Experimental and theoretical results show the linear dependency (which depends on the refining degree) of the standard pore radii and mean pore radius.

Series of eucalyptus handhseets were prepared with different refining degrees, different grammages. The experimental results reported in [1,96,95,97] were deduced from a capillary flow porometer. Then we performed granulometry measurements on bulk. The results are presented in Figure 24. These curves represent the relative volume frequency as a function of pore radius.

The characteristics of theses curves are summarised in Table 11. The maximum pore size is defined, in our case, as the mean radius of the 5% of the largest pores.

We first checked that the pore size distribution follows the model referred above.

At the observation scale, Table 11 does not indicate significant changes in the mean pore radius and in the maximum pore radius with changes in grammage, in refining degree and in the pressing in the bulk. This does not correspond to the models found in the literature: Dodson [97] found an

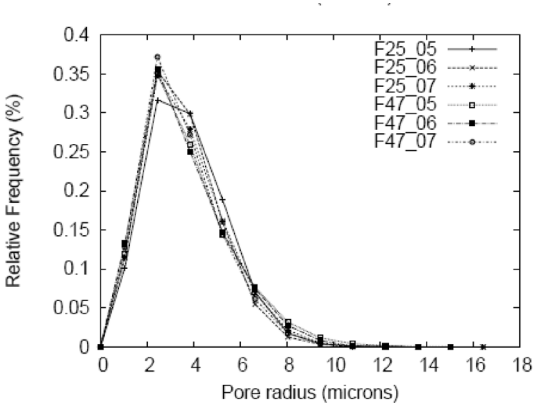

Figure 24. Pore size distribution. F referes to hardwood samples (eucalyptus), 25 or 47 to the refining degree in °SR and 05, 06 and 07 to different weights (g) of the handsheets.

Table 11. Characteristics of the granulometries. The magnitudes are reported in microns.

Sample	*mean pore radius*	*standard deviation*	*maximum pore radius*
F25_05	3.69	1.68	7.39
F25_06	3.68	1.60	7.14
F25_07	3.59	1.71	8.04
F47_05	3.68	1.94	8.74
F47_06	3.57	1.84	7.36
F47_07	3.44	1.67	7.81

increase of both quantities with a decrease of the grammage. However it is more coherent with experimental results reported by Urquhart [95] who found that the mean pore radius is independent of the grammage for unbeaten samples and decreases with increasing grammage for beaten samples. This can come from the fact that the biggest pores are located in the boundary layers and not in the bulk.

We investigated the link between standard deviation of pore radii with mean pore radius [97,96]. Analysing the plots of the standard deviation of pore radii (std(r)) versus the pore mean radius ($\bar{r}$), their fits were obtained for two given refining degrees: 26°SR and 47°SR. The fits were, respectively:

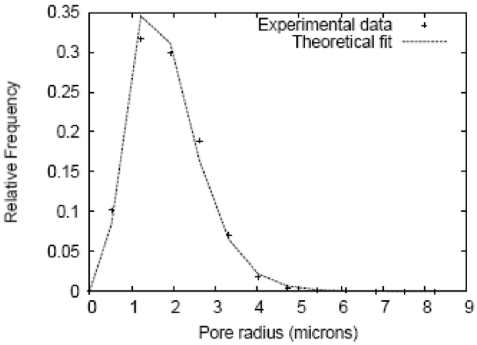

Figure 25. Example of frequency distribution of pore radii (dots) and its fit to the gamma distribution (line) for a sample.

std(r) = 0.49.r – 0.05 and std(r) = 0.50.r – 0.03. The coefficients of determination for the last three fits were 90% and 75%, respectively. These relations seem to be in agreement with the developed models and experimental results found in the literature [97,96].

Conclusion

The study concerned only the characterisation of the pore phase in the bulk. The distribution of pore sizes can be estimated either in 2D or in 3D and are characterised by their mean, maximum and standard deviation. This comparison indicated a good agreement between models and experimental results when models or experimental results reported in the literature involves the mean pore sizes. Nevertheless, when models require 3D measures of the pore size, we did not always find a good agreement between the literature results and our experimental results obtained only in the bulk. This can be due to the fact that the chosen resolution was not adapted and a higher one may have to be considered. This might have been due to the fact that the results presented in this section are not carried out in the surface layers which play a crucial role in the pore size distribution. The comparison between the pore height distribution obtained on the microtomographic data and the proposed ones in the literature showed nevertheless a good agreement. It demonstrates also the complementarities between theoretical and experimental results.

IN SITU 3D STRUCTURE EVOLUTION

The aim of this chapter is to describe the evolution of the fibrous structure due either to an applied stress or a modification of humidity. We focus on the feasability of the experimental technique to visualise the induced modifications in 3D in the case of paper. The complete review of the modelling of these physical phenomena is beyond the scope of this article. The interested reader may refer to [99–101].

Influence of compression on the sheet structure

Compression happens in paper life time during the production (for example during calendering) or during its use (for example during printing). Two types of compression occur during paper deformation: a reversible one and an irreversible one. Few works related the effect of compression on the paper and board structures. For example, Rodal [102] proposed to decompose the paper compression during calendaring in the thickness direction in three major mechanisms. The first stage involves the reduction of the pore volume in the sheet. The second stage involves elastic-plastic buckling of the fibre walls. The final stage involves the crushing of the fibres. Kananen, [103], in this conference in 2001 carried out a detailed study on the effect of the grammage and of each paper constituents (types of fibre, kinds of pulp, amount of fines and presence of fillers) in the case of reversible compression. He found that porosity mostly influences the effective elastic modulus.

Analysing the effect of compression by synchrotron XRM was already successfully carried out on fibrous media in the case of felts by Thibault in 2001 [44]. These pioneer experiments allowed us to develop compression devices which are currently improved in the context of papermaking.

Experimental results

The analysed sample is placed in the compression device. It is set between two pistons. The bottom one is fixed whereas the top one can be moved vertically by a micrometric screw system. To avoid the sample being sheared while compressed, a small ball is inserted between the top cylinder and the micrometric screw. A Plexiglas tube guides the cylindrical element described above.

In the presented example, four deformation levels were applied on a blotting paper. The first one corresponds to the so-called reference level. Figure 26 shows the different compression levels imposed. The four consecutive levels are referred as level0, level1, level2 and level3, respectively. These results validate the feasibility of such a study from the experimental point of view.

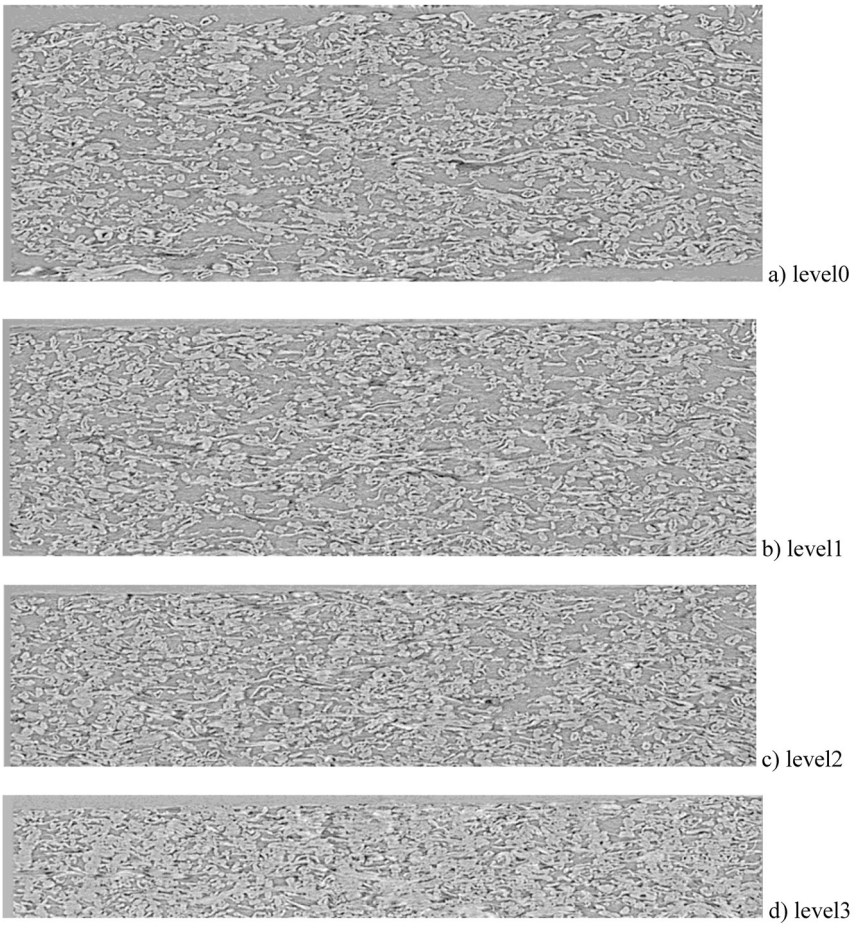

Figure 26. Thickness slices of the different compression levels applied to the blotting paper. All the images are 1.4 mm in width and they are from top to bottom 0.491 mm, 0.442 mm, 0.392 mm and 0.274 mm in height.

The next step is to characterise the micro structural evolution during compression.

Micro structural analysis

Quantitative structural analysis can be carried out on the microtomographic data as the imaged volume is larger than the Representative Elementary

Volume. The data are obtained on the segmented data presented in the case of the blotting paper under deformation.

Table 12 presents the obtained results on both porosity and thickness for the four different levels. The porosity is evaluated on the segmented data and the thickness is directly measured on the radiographs.

The thickness and porosity variations were evaluated by evaluating the following quantities:

$$\Delta t = \frac{t - t_0}{t_0} \tag{21}$$

Where Δt represents the thickness of the considered level and t_0 the thickness of the reference level.

Table 13 presents the obtained results for the deformation characterisation.

A simple analysis may be carried out. Porosity and thickness variations were evaluated. For level1, the porosity and thickness variations have the same order of magnitude which corresponds to the pore compressions. But it can also be underlined that for the two last compression levels, the thickness variations and the porosity variations are not equal any more. This means that the compression modifies the sizes of both pores and fibres. This behaviour is confirmed by the study of the porosity profiles presented in Figure 27. These profiles are presented twice, as they give complementary information. The first one presents the porosity versus the true thickness and the second the porosity versus the dimensionless thickness. On these graphs,

Table 12. Thickness and porosity of the four compression levels evaluated on the microtomographic data.

	Level0	*Level1*	*Level2*	*Level3*
Thickness [μm]	491	442	392	272
Porosity [%]	69	62	60	49

Table 13. Characterisation of the deformation [41].

	Level0	*Level1*	*Level2*	*Level3*
Thickness variation		0.10	0.20	0.44
Porosity Variation		0.10	0.13	0.29

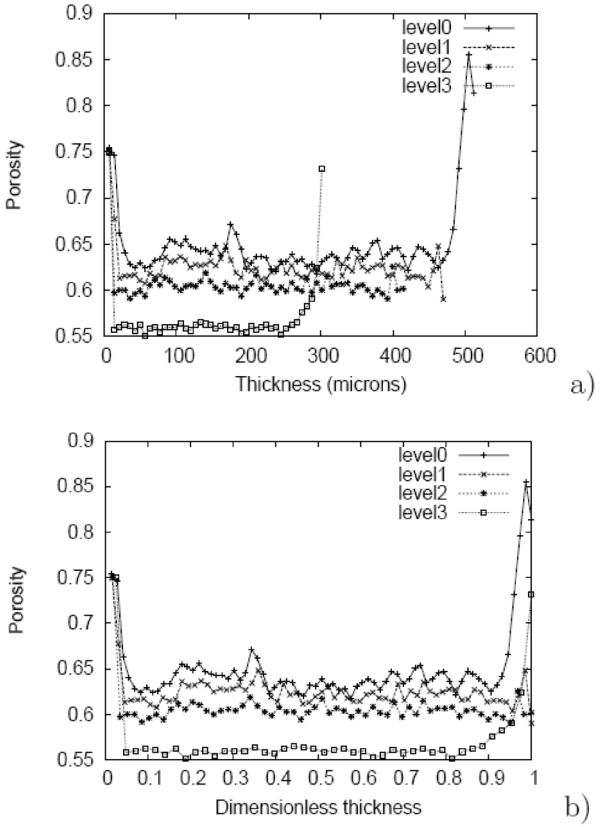

Figure 27. Porosity profiles for the four deformation levels of the blotting paper. The porosity is averaged on 7 μm. The top graph a) presents the porosity versus the thickness and the bottom one b) the porosity versus the dimensionless thickness.

the porosity is averaged on 10 slices that is to say on 7 microns. The pressure is applied by the cylinder located at the top of the sample. The origin of these graphs corresponds to the bottom of the sample.

As expected the mean value of porosity decreases as the applied pressure increases. The porosity variations around the mean value for each deformation level are also interesting. We can notice that the top layers (more than 300 μm) are smoothed earlier than the bottom ones in term of porosity variations. It leads therefore to a heterogeneous deformation. Moreover, it can be remarked that the porosity profile of level1 can be deduced from level0 porosity profile by a simple translation of porosity (0.04). This may confirm that the first deformation level only affects the pores.

The comparison between the level2 and the two previous porosity profiles shows that only the highest peaks of the variations of porosity around the mean remain. This may come from the fact that the fibres start to be compressed. The last profile is flat, the variations around the mean porosity being smaller than one point. The disappearance of the porosity variations can be linked to the compression of both pores and fibres. The compression of fibres is confirmed by the experimental evaluation of the irreducible thickness as a relative difference of 20% between the experimental (level4) and the theoretical one demonstrates it. These profiles also show that the two first compression levels (level1 and level2) affect mainly the paper surface as the major variation in porosity can be observed in this zone. Finally, no lateral movement of fibres was detected when following the trajectory of a few selected fibres during compression (uniaxial deformation of paper).

The next step is to evaluate the modification of the structure during various mechanical influences such as tensile tests. This was already published for other materials [62] but is still in development concerning paper samples.

Influence of humidity on paper structure

Position of the problem

Hygro expansion is a classical property of interest for paper scientists. Some interesting studies, such as [104], may be cited. However, studies of the influence of humidity on micro structure are scarcer. The resolution reached in synchrotron facilities (ESRF, for example) can be less than one micron. Such a high resolution requires specific attention to external factors that can blur data during acquisitions such as mechanical vibration or thermal variations. The higher the resolution is, the more crucial is the role of environmental conditions. In the case of paper grades, they were initially successfully imaged by synchrotron X-ray microtomography in absorption mode at a pixel size of 2 microns at the European Synchrotron Radiation Facility on ID19 [39]. However, when decreasing the pixel size to less than one micron as currently carried out, paper samples data can be blurred [105]. Namely, image quality in term of edge definitions is lower than the one obtained on other fibrous materials such as felt or filters made of synthetic fibres at the same resolution. On the other hand, Holmstadt [48] correlated the basis weight of paper samples obtained by β radiography and by X-ray tomography. He found a difference of about 10 $g.m^{-2}$ for grammages between 45–65 $g.m^{-2}$. He suggested that this loss of mass comes from the sample preparation and from the missing fines as they are smaller than the resolution. However at least part of these particles attenuates enough the beam to induce a variation of the

transmitted beam. This loss of mass can also arise from the drying of the sample during the scan. Namely the beam might dry the sample during data acquisitions inducing dimensional changes, blurring the data [106].

To overcome this problem linked to sample structure modifications during data acquisitions, we developed a sample environment to control the local environment of the paper during data acquisitions. This consists in a controlled wet air generator placed near the sample. It allows the stabilisation of the sample structure during the data acquisition. The stabilisation of the paper is obtained for a given relative humidity (RH) condition. The wet air generator is also used to study the influence on the structure of a cycle of RH rates. Therefore, the hygro-expansion which is defined as the dimensional change due to the change in internal moisture may be studied. It is due to the swelling, or contraction, of the fibrous structure when their moisture content changes. Therefore paper expands when the dimensional changes of fibre are transferred to the dimensions of the macroscopic network [107]. This depends on the hygro-expansion of a single fibre and on the efficiency of the stress transfer from the network to the fibres [104]. Namely the dimensional changes in one direction can directly be related to the intercept number in this direction and the mean variation of the fibre diameter [108]. Therefore the main problem is to analyse qualitatively and quantitatively the dimensional changes of samples due to a humidity cycle by Synchrotron radiation microtomography. To investigate these phenomena, a pixel size of 0.7 micron was chosen. The imaged volumes were found to be suitable to study such phenomena [41].

Sample environment dedicated to humidity study

Figure 28 represents a picture of the sample environment installed around the microtomograph. The wet air generator consists in a compressed air pretreatment device and a control unit. These two elements were installed in the control room. The output of the wet air generator was placed in front of the analysed sample in the experimental room. As the generated wet air had to go through about 10 meters in a tube before being delivered, we checked that the humidity output and the regulating one are identical. Therefore a control humidity sensor was placed in front of the output of the generator, after the sample. When installing the set-up around the microtomograph, we paid attention that the motion induced by the generated air flow did not make the sample vibrate. Hence, the distance between the output and the sample was about 20 cm and can be down to 5 cm.

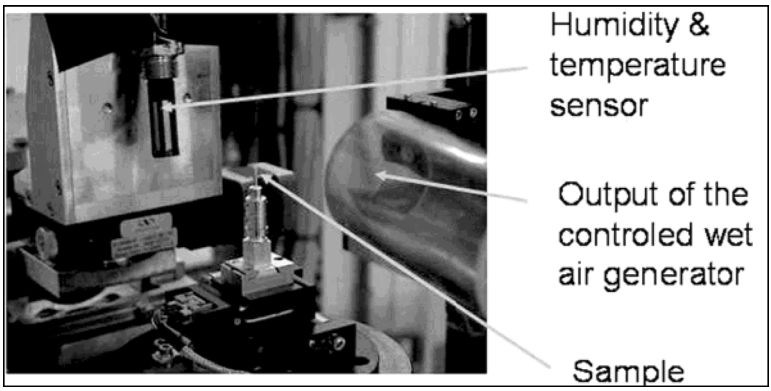

Figure 28. Picture of the experimental set-up to control the humidity around the microtomograph [41].

Experimental protocol

Scans are therefore performed for different samples under a cycle of humidity rates: 50%, 20%, 80%, 20% and 50. The diffusion time of moisture into paper depends on the basis weight [109]. For low basis weight paper, the diffusion time is proportional to the basis weight whereas it is proportional to the squared basis weight for high basis weight. Therefore preliminary measurements were carried out on the studied samples using the varidim® apparatus. It consists in a commercial laboratory equipment that measures length variations for different humidity rates. The wet air generator was the same as the one used during our microtomographic acquisitions. The humidity levels are imposed during two hours. The dimensional changes are recorded as a function of time. It appeared that all the main dimensional changes occur during the first 15 minutes. Furthermore, the samples analysed are much larger (10 cm × 1 cm) than the one measured with microtomography (1.5 mm × 1.5 mm). Therefore the sample was 'humidified' for about 5 minutes before scanning in order to avoid dimensional changes during the scan for any humidity rate. The samples were directly glued on a cylinder to get a fixed reference. The following pictures illustrate in the case of a tracing paper, the modification of the 3D structure. The evolution of a single layer extracted from the 3D structure is presented.

The visual inspection of samples proved that the evolution of the macroscopic 3D structure was due in a part to a modification of the structure of the fibre itself and that this behaviour may be studied using XRM.

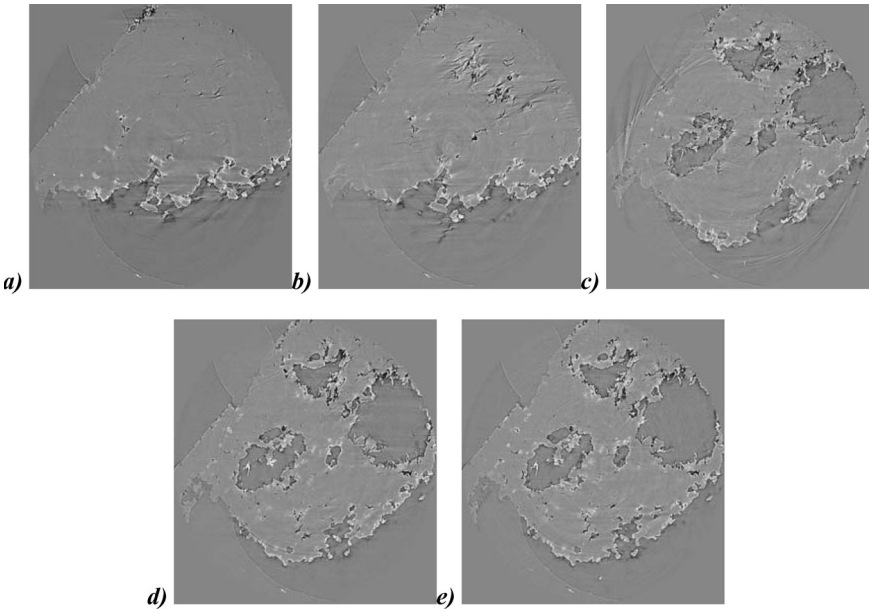

Figure 29. Influence of humidity on tracing paper: in-plane slices (1.4 mm × 1.4 mm) at the same vertical position. a), b), c), d) and e) represent the slices for the successive humidity rates that are 50%, 20%, 80%, 20% and 50%, respectively [41].

CONCLUSIONS

The main conclusions of the presented works may be summarized as follow:

- The determination of the Representative Elementary Volume dedicated to geometry of paper structures validates *a posteriori* all the published data obtained from X-Ray Microtomography in order to describe the fibrous structure.
- The description of the 3D structure was proved to be obtained in a quantitative way. The last evolutions in term of 3D structure analysis lead to structural mean parameters.
- The need to obtain 3D quantification of the paper structure for both mean values and also their variations is clear. This is of course, a major improvement that was not possible few years ago due to the lack of technical or computing solutions.
- The complementary aspects of experimental measurement and theories were demonstrated.

PERSPECTIVES

The perspectives may be divided into two main points: The structure characterization and its modification due to changes of the so-called environment (temperature, humidity, deformation . . .).

Structural characterisation

- The structural characterisation of paper sample was carried out in a quantitative way. However, the next step will be to introduce the variation of such parameters at a given geometrical scale but also at different scales. For instance, the formation may be studied in this sense taking into account the heterogeneity of paper. Concerning the further structural analysis, a key point would be to skeletonise either the pore phase of the fibre phase in an automatic way, which does not exist nowadays. It will be a step towards the improvement concerning the influence of connectivity on physical properties.
- The comparison of the simulated network to the microtomographic data can help to validate softwares, such as [110] or [111]. In parallel, the development of simulation tools to calculate physical properties of paper samples (for examples [14], [47] or [112],) taking into account the microstructure can lead to the optimisation of paper materials. Synchrotron X-Ray imaging and new microtomes appear as key tools to validate, or not, these models.
- The contact area distribution is a key factor to be evaluated either theoretically or experimentally in order to estimate the mechanical properties for example. However, it is vain to search for a direct determination of the mechanical properties from the structure itself, as no unique relationship exists between the structure and the mechanical properties, which may be strongly modified by a change of humidity or temperature for examples. The possibility to evaluate this property directly on an industrial paper is also of main importance.

Microstructure analysis coupled with sample environments

We showed that microtomography of paper samples can be coupled with dedicated sample environments such as compression device or humidity regulation. The humidity set-up opens the possibility of a detailed study of phenomena linked to the hygro-expansion of paper when moisture content changes. It induces dimensional changes of paper samples that may be evaluated. This behaviour is actually considered in 3D. The compression set-up

gives the opportunity to investigate the fibres and the pores behaviours when compressed. Furthermore, many other mechanical tests may be carried out at this microscopic scale, taking into account the influence of humidity. It will allow also the detailed investigation of the physical properties such as permeability, including the influence of the deformation. The increasing ability of the measurement system, and in particular both the pixel size and the acquisition velocity, will also lead to studies dedicated to 'quasi-statics' evolutions of phenomena. The coupling of pore size and mass distribution may also lead to the modelling of the distribution of optical properties which are obviously important for paper.

ACKNOWLEDGMENTS

The authors wish to acknowledge C. Geindreau and L. Orgeas for their scientific help during all these years, P. Dumont and W. Sampson for the corrections on the manuscript.

REFERENCES

1. Sampson W. W. The Structural Characterisation of Fibre Networks in Papermaking Processes – A Review. In **The Science of Papermaking**, *Trans. 12th Fund. Res. Symp. Oxford 2001* (C. F. Baker, ed.), pp. 1205–1288, FRC, Manchester, 2001.
2. Corte H. and Kallmes O. J. Statistical geometry of a fibrous network. In **The Formation and Structure of Paper**, *Trans 2nd Fund. Res. Symp. Oxford, 1961* (F. Bolam, ed.), pp. 13–46, FRC, Manchester, 2003.
3. Sampson W. W. **Modelling Stochastic Fibrous Materials with Mathematica**, Springer, 2009.
4. Deng M. and Dodson C. **Paper- An Engineered Stochastic Structure**, Tappi Press, 1994.
5. Ohser J. and Mucklich F. **Statistical Analysis of Microstructures in Materials Science**, John Wiley and Sons, 2000.
6. Torquato S. **Random Heterogeneous Materials – Microstructure and Macroscopic Properties**, Springer, 2002.
7. Sone T. Tamada T. Jo Y. Miyoshi H. and Fukunaga M. Analysis of three-dimensional microarchitecture and degree of mineralization in bine metastases from prostate cancer using synchrotron microcomputed tomography, *Bone*, **35**, pp. 432–438, 2004.
8. Jones A. Sheppard A. P. Sok R. M. Arns C. H. Limaye A. Averdunk H. Brandwood A. Sakellariou A. Senden T. J. Milthorpe B. and Knackstedt M. A. Three-dimensional analysis of cortical bone structure using X-ray micro-computed tomography, *Physica A*, **339**, pp. 125–130, 2004.

9. Arns J. Robins V. Sheppard A. P. Sok R. M. Pinczewski W. V. and Knackstedt M. A. Effect on Network Topology on relative Permeability, *Transport in Porous Media*, **55**, pp. 21–46, 2004.
10. Al-Raoush R. I. and Willson C. S. Extraction of Physically Realistic Pore Network Properties from Three Dimensional Synchrotron X-Ray Microtomography Images of Unconsolidated Porous Media Systems," *Journal of Hydrology*, **300**, pp. 44–64, 2005.
11. Kortschot M. The role of the fibre in the structural hierarchy of paper, In **The Fundamentals of Papermaking Materials**, *Trans 11th Fund. Res. Symp. Cambridge 1997* (C. F. Baker, ed.), pp. 351–399, FRC, Manchester, 2003.
12. Jaganathan S. Vahedi Tafreshi H. and Pourdeyhimi B. A realistic approach for modeling permeability of fibrous media: 3-D imaging coupled with CFD simulation, *Chemical Engineering Science*, **63**(1), pp. 244–252, 2008.
13. Jaganathan S. Vahedi Tafreshi H. and Pourdeyhimi B. 2008, Modeling liquid porosimetry in modeled and imaged 3-D fibrous microstructures, *Journal of Colloid and Interface Science*, **326**(1), pp. 166–175, 2008.
14. Koivu V. Mattila K. Alaraudonjoki J. Kataja M. Decain M. Bloch J. and Geindreau C. Flow permeability of fibrous porous materials. Micro-tomography and numerical simulations, In **Advances in Pulp and Paper Research**, *Trans. 14th Res. Fund. Symp. Oxford 2009* (S.J. I'Anson, ed.), FRC, Manchester, 2009.
15. Torquato S. Theory of Random Heterogeneous Materials, **Handbook of Materials Modeling**, Springer, pp. 1333–1357, 2005.
16. Levitz P. Toolbox for 3D imaging and modeling of porous media: Relationship with transport properties, *Cement and Concrete Research*, **37**, pp. 351–359, 2007.
17. Sok R. M. Knackstedt M. A. Sheppard A. P. Pinczewski W. Lindquist W. Venkatarangan A. and Paterson L. Direct and Stochastic Generation of Network Models from Tomographic Images; Effect of Topology on Residual Saturations, *Transport in Porous Media*, **46**(2), pp. 345–371, 2002.
18. Torquato S. Modeling of physical properties of composite materials, *International Journal of Solids and Structures*, **37**(1–2), pp. 411–422, 2000.
19. Manwart C. Torquato S. and Hilfer R. Stochastic reconstruction of sandstones, *Phys. Rev. E*, **62**(1), p. 893, 2000.
20. Chinga-Carrasco G. Kauko H. Myllys M. Timonen J. Wang B. Zhou M. and Fossum J. O. New advances in the 3D characterization of mineral coating layers on paper, *Journal of Microscopy*, **232**(2), pp. 212–224, 2008.
21. Turpeinen T. Laheteela A. Myllys M. Kataja M. and Timonen J. Computerized Tomographic Imaging of Paper Coating Layer. *Chemical Technology of papermaking Symposium*, Munich, Germany, pp. 1–17, 2004.
22. Sakellariou A. Arns C. H. Sheppard A. Sok R. Averdunk H. Limaye A. Jones A. Senden T. and Knackstedt M. Developing a virtual materials laboratory, *Materials today*, **10**(12), pp. 44–51, 2007.
23. Dobrich K. M. Rau C. and Krill C. E. Quantitative characterization of the three-dimensional microstructure of polycrystalline Al-Sn using X-ray microtomo-

graphy, *Metallurgical and Materials Transactions A-Physical Metallurgy and Materials Science*, **35A**(7), pp. 1953–1961, 2004.
24. Wongs P. E. A. **Methods in the Physics of Porous Media**, Academic Press, 1999.
25. Wiltsche M. Three-dimensional analysis of paper structure with an automatic microtome, PhD thesis, University of Graz, Austria, 2006.
26. Delisee C. Jeulin D. and Michaud F. Caractérisation morphologique and porosité en 3D de matériaux fibreux cellulosiques, *Compte-Rendus de l'Académie des Sciences*, Paris, France, **329**, pp. 179–185, 2001.
27. Aronsson M. On 3D Fibre measurements of digitized paper, From microscopy to Fibre network. PhD, Swedish University of Agricultural sciences, Uppsala, Sweden, 2002.
28. Niskanen K. and Rajatora H. Statistical geometry of Paper Cross-Sections, *Journal of Pulp and Paper Science*, **28**(7), pp. 228–233, 2002.
29. Aronsson M. Henningsson O. and Savborg O. Slice-based digital volume assembly of a small paper sample. *Nordic Pulp and Paper Research Journal*, **17**(1), pp. 29–33, 2002.
30. Wiltsche M. Donoser M. Bauer W. and Bischof H. A new slice-based concept for 3D paper structure analysis applied to spatial coating layer formation. In **Advances in Paper Science and Technology**, *Trans 13th Fund. Res. Symp. Cambridge 2005* (S. J. I'Anson, ed.), pp. 853–899, FRC, Manchester, 2005.
31. Alarousu E. Krehut L. Prykari T. and Myllyla R. Study on the use of optical coherence tomogrpahy in measurements of paper properties, *Measurement science and technology*, **16**, pp. 1–7, 2005.
32. Selomulya C. Jia X. and Williams R. Direct prediction of structure and permeability of flocculated structures and sediments using 3D tomographic imaging, *Chemical Engineering Research and Design*, **83**(A7), pp. 844–852, 2005.
33. Rolland du Roscoat, S. Bloch J. and Thibault X. Characterisation of the 3D paper structure with X-Ray Synchrotron radiation microtomography. In **Advances in Paper Science and Technology**, *Trans 13th Fund. Res. Symp. Cambridge 2005* (S. J. I'Anson, ed.), pp. 901–920, FRC, Manchester, 2005.
34. Baruchel J. Buffière J. Maire E. Merle P. and Peix G. **X-Ray tomography in material science**, Hermes, 2005.
35. Ramaswamy S. Huang S. Goel A. Cooper A. Choi D. Bandhyopadhyay, A. and Ramarao B. The 3D structure of paper and its relationship to moisture transport in liquid and vapour forms, The Science of Papermaking, Oxford, UK, pp. 1289–1311, 2001.
36. Goel A. Tzanakakis M. Huang S. Ramaswamy S. Choi D. and Ramarao B. Characterization of the three-dimensional structure of paper using X-ray microtomography, *Tappi J.* **84**(5), 2001.
37. Samuelsen E. Gregersen O. Houen P. and Helle T. Three-dimensional imaging of paper by use of synchrotron X-ray microtomography, *International Paper Physics Conf.* Tappi, Victoria, Canada, p. 307, 1999.
38. Gureyev T. Evans R. Stevenson A. Gao D. and Wilkins S. X-ray phase contrast microscopy of paper, *Tappi J.* **84**(2), 2001.

39. Reverdy-Bruas N. Serra-Tosio J. Bloch J. and Boller E. Caractérisation de papier avec la microtomographie au rayon X. *Association Technique de l'Industrie Papetière*, **55**(4), pp. 12–18, 2001.
40. Reverdy-Bruas N. Contribution à l'étude des propriétés physiques des structures fibreuses compressibles. Cas particulier du pressage à impulsion thermique en papèterie, PhD, Institut National Polytechnique de Grenoble, France, 2002.
41. Roscoat S. R. D. Contribution à la Quantification de Réseaux Fibreux par Microtomographie au Rayonnement Synchrotron : Applications aux Papiers, PhD, Institut National Polytechnique de Grenoble, 2007.
42. Holmstad R. Aaltosalmi U. Ramaswamy S. Kataja M. Koponen A. Goel A. and Gregersen O. Comparison of 3D structural characteristics of high and low resolution X-Ray microtomographic images of paper, *Nordic Pulp and Paper Research Journal*, **20**(3), pp. 283–288, 2005.
43. Axelsson M. Image Analysis for Volumetric Characterisation of Microstructure, PhD, Swedish University of Agricultural sciences, Uppsala, Sweden, 2009.
44. Thibault X. and Bloch J. F. 2002, Structural analysis by X-ray microtomography of a strained nonwoven papermaker felt, *Text. Res. J*, **72**(6), pp. 480–485, 2002.
45. Thibault X. Bloch J. F. and Boller E. "Felt structure characterised by synchrotron microtomography, *Appita Journal*, **55**(2), pp. 145–148, 2002.
46. Peralba M. Dumont P. Bloch J.-F. Dubé M. Mangin P. Rolland du Roscoat S. and Geindreau C. Influence of structure and wear of paper forming fabrics on their permeation properties, *Second World Conf. on 3D Fabrics and their applications*, April 6–7, 2009, Greenville, South Carolina, USA, p. 12,, 2009.
47. Rolland du Roscoat S. Decain M. Thibault X. Geindreau C. and Bloch J. Estimation of microstructural properties from synchrotron X-ray microtomography and determination of the REV in paper materials, *Acta Materialia*, **55**(8), pp. 2841–2850, 2007.
48. Holmstad R. Methods for paper structure characterisation by means of image analysis, PhD, NTNU, Norway, 2004.
49. Defrenne Y. Zhankin Z. Ramaswamy S. and Ramarao B. Improved method to visualize and characterize high resolution X-Ray Micro-Tomographic images of paper and board. *Progress in Paper Physics – A seminar*, US, pp. 65–66, 2006.
50. Antoine C. Nygard P. Holmstad R. Gregersen O. Weitkamp T. Rau C. Solheim O. and P. Houen, Binarisation of 3D images of paper obtained by phase-contrast x-ray microtomography. *COST Action E11, Final Workshop*, Espoo, Finland, 2001.
51. Underwood E. E. **Quantitative Stereology**, Addison Wesley, 1969.
52. Matheron G. **Eléments pour une théorie des milieux poreux**, Masson, 1967.
53. Masse J. Salvo L. Rodney D. Brechet Y. and Bouaziz O. Influence of relative density on the architecture and mechanical behaviour of a steel metallic wool, *Scripta Materialia*, **54**, pp. 1379–83, 2006.
54. Jeulin D. **Homogénéisation en mécanique des matériaux**, Hermès, 2001.
55. Silvy J. Etude structurale de milieux fibreux : cas des fibres cellulosiques." PhD, Institut National Polytechnique de Grenoble, France, 1980.

56. Silvy J. Caret C. Belamaalen B. and Mahrous M. The three-dimensional structure of paper: methods of analysis and implications on its physical properties, *International Paper Physics Conference*, Niagara-on-the-Lake, Canada, 1995.
57. Bloch J. F. and Champon G. "Anisotropy of paper: Comparison of different laser tools, *Optical Diagnostic Methods For Inorganic Materials II*, L.M. Hanssen, ed. SPIE-Int Soc Optical Engineering, pp. 106–115, 2000.
58. Drouin B. Gagnon R. Schroder A. Butel M. and Silvy J. L'orientation des fibres and les propriétés mécaniques du papier: méthodes de contrôle de l'anisotropie de la feuille, *ATIP*, **49**(2), pp. 66–71, 1995.
59. Holmstad R. Antoine C. Gregersen O. Nygard P. Silvy J. and Costa A. Verification of the equivalent pore model using 3D paper, *COST Action E11*, 2001.
60. Holmstad R. Antoine C. Silvy J. Costa A. and Antoine J. Modelling the paper sheet structure according to the equivalent pore concept, *COST Action E11, Final Workshop*, Espoo, Finland, 2001.
61. Silvy J. and Butel M. Filtration laws and small scale investigations of fibres-mats, *Final report JOU 2 CT 92-OO4, C.E.E*, 1996.
62. Buffiere J. Maire E. Verdu C. Cloetens P. Pateyron M. Peix G. and Baruchel J. Damage assessment in an Al/SiC composite during monotonic tensile tests using synchrotron X-ray microtomography, *Materials Science and Engineering A*, **234–236**, pp. 633–635, 1997.
63. Dodson C. On the distribution of pore heights in random layered fibre networks, Oxford, In **The Science of Papermaking**, *Trans. 12th Fund. Res. Symp. Oxford 2001* (C. F. Baker, ed.), pp. 1037–1042, FRC, Manchester, 2001.
64. Lin C. and Miller J. 3D characterization and analysis of particle shape using X-ray microtomography (XMT), *Powder Technology*, **154**, pp. 61–69, 2005.
65. Wang L. and Ramaswamy S. Surface Structure characterization of Porous Materials Using X-Ray Micro-Computed Tomography. *The 2004 Progress in Paper Physics Seminar*, Norway, 2004.
66. Spanne P. Thovert J. F. Jacquin C. J. Lindquist W. B. Jones K. W. and Adler P. M. Synchrotron Computed Microtomography of Porous Media : Topology and Transports, *Physical Review Letters*, **73**, pp. 2001–2004, 1994.
67. Geandier G. Hazotte A. Denis S. Mocellin A. and Maire E. Microstructural analysis of alumina chromium composites by X-ray tomography and 3-D finite element simulation of thermal stresses, *Scripta Materialia*, **48**, pp. 1219–1224, 2000.
68. Buffière J. Maire E. Cloetens P. Lenormand G. and Fougeres R. Characterisation of internal damage in a MMC using X-Synchrotron phase contrast microtomography, *Acta Materialia*, **47**(5), pp. 1613–1625, 1999.
69. Kanit T. Forest S. Galliet I. Mounoury V. and Jeulin D. Determination of the size of the representative volume element for random composites: statistical and numerical approach, *International journal of solids and structure*, **40**, pp. 3647–3679, 2003.
70. Stroeven M. Askes H. and Sluys L. Numerical determination of representative volumes for granular materials, *Computer methods in applied mechanics and engineering*, **193**, pp. 3221–3238, 2004.

71. Hill R. Elastic properties of reinforced solids: some theoretical principles, *Journal of the mechanics and Physics of Solids*, **11**, pp. 357–372, 1963.
72. Drugan W. and Willis J. A micromechanics-based nonlocal constitutive equation and estimates of representative volume element size for elastic composites, *Journal of the mechanics and physics of solids*, **44**(4), pp. 497–524, 1996.
73. Gusev A. Representative volume element size for elastic composites: a numerical study, *Journal of the mechanics and physics of solids*, **45**(9), pp. 1449–1459, 1997.
74. Ostoja-Starzewski M. Materials spatial randomness: from statistical to representative volume element, *Probabilistic Engineering mechanics*, **21**, pp. 112–132, 2006.
75. Kanit T. N'Guyen F. Forest S. Jeulin D. Reed M. and Singleton S., Apparent and Effective Physical Properties of Heterogeneous Materials: Representativity of Samples of two Materials from Food Industry, *Comp. Methods Appl. Mech. Eng.*, **195**(33–36) pp. 3960–3982, 2006.
76. Zhang D. Zhang R. Chen S. and Soll W. Pore scale study of flow in porous media: Scale dependency, REV and statistical REV, *Geophysical Research Letters*, **27**, pp. 1195–1198, 2000.
77. Jeulin D. Estimation of the point variance of the Specific Surface Area, *Note interne du Centre de Morphologie Mathématique*, 2006.
78. Hazlett R. Statistical Characterization and Stochastic Modeling of Pore Networks in Relation to Fluid Flow, *Mathematical Geology*, **29**(6), pp. 801–822, 1997.
79. Hazlett R. D. Simulation of capillary-dominated displacements in microtomographic images of reservoir rocks, *Transport in Porous Media*, **20**(1), pp. 21–35, 1995.
80. Arns C. H. Knackstedt M. A. Pinczewski W. V. and Martys N. S. Virtual permeametry on microtomographic images, *Journal of Petroleum Science and Engineering*, **45**(1–2), pp. 41–46, 2004.
81. Singh R. Lavrykov S. and Ramarao B. V. Permeability of pulp fiber mats with filler particles, *Colloids and Surfaces A: Physicochemical and Engineering Aspects*, **333**(1–3), pp. 96–107, 2009.
82. Bernard D. Nielsen O. Salvo L. and Cloetens P. Permeability Assessment by 3D Interdendritic Flow Simulations on Microtomography Mappings of AL-Cu Alloys, *Materials Science and Engineering A*, **392**, pp. 112–120, 2005.
83. Ingmanson W. L. and Thode E. Factors Contributing to the Strength of a Sheet of Paper. II. Relative Bonded Area, *Tappi J.* **42**(1), pp. 83–93, 1959.
84. Swanson J. and Steber A. Fiber Surface Area and Bonded Area, *Tappi J.* **42**(12), pp. 986–994, 1959.
85. Hazelton W. Gas Adsorption by Wood, Pulp, and Paper, I. The low-Temperature Adsorption of Nitrogen, Butane, and Carbone Dioxide by Sprucewood and its components, *Tappi J.* **37**(9), pp. 404–412, 1954.
86. Hazelton W. Gas Adsorption by Wood, Pulp, and Paper, II. The Application of Gas Adsorption techniques to the Study of the Area and Structure of Pulps and the Unbonded and Bonded Area of Paper, *Tappi J.* **38**(12), pp. 716–723, 1955.

87. Luner P. Karna A. and Donofrio C. Studies in Interfiber Bonding of Paper, *Tappi J.* **44**(6), pp. 409–414, 1961.
88. Kallmes O. J. and Eckert C. The Structure of Paper – VII – The application of the Relative Bonded Area Concept to Paper Evaluation, *Tappi J.* **47**(9), pp. 540–548, 1964.
89. Skowronski J. Fibre-to-Fibre Bonds in Paper. Part II: Measurement of the Breaking Energy of Fibre-to-Fibre Bonds, *JPPS*, **17**(6), pp. 217–222, 1991.
90. Soszynski R. Relative bonded area – A different approach," *NPPRJ*, **2**, p. 150, 1995.
91. Batchelor W. and He J. A new method for determining the relative bonded area, *Tappi J.* **4**(6), pp. 23–28, 2005.
92. He J. Batchelor W. and Johnston R. An analytical model for number of fibre-fibre contacts in paper and expressions for relative bonded area (RBA), *J. Mater. Sci.* **45**, pp. 522–528, 2007.
93. Sampson W. A model for fibre contact in planar random fibre networks, *J. of Material Science*, **39**, pp. 2775–2781, 2004.
94. Batchelor W. He J. and Sampson W. Inter-fibre contacts in random fibrous materials: experimental verification of theoretical dependence on porosity and fibre width, *J. Material Science*, **41**, pp. 8377–8381, 2006.
95. Urquhart S. Experimental and theoretical analysis of factors affecting the pore size distribution of paper, PhD, University of Manchester, U.K, 2006.
96. Roberts S. and Sampson W. The pore radius distribution. Part II: the effect of laboratory beating, *Appita J.* **56**(4), pp. 281–289, 2003.
97. Dodson C. Handley A. Oba Y. and Sampson W. The pore radius distribution in paper. Part I: the effect of formation and grammage, *Appita J.* **56**(4), pp. 275–280, 2003.
98. Dodson C. and Sampson W. The effect of paper formation and grammage on its pore size distribution, *Journal of Pulp and Paper Science*, **22**(5), pp. J165-, 1996.
99. Maire E. Fazekas A. Salvo L. Dendievel R. Youssef S. Cloetens P. and Letang J. X-Ray Tomography Applied to the Characterization of Cellular Materials. Related Finite Element Modeling Problems, *Composites Science and Technology*, **63**, pp. 2431–2443, 2003.
100. Jaganathan S. Vahedi Tafreshi H. Shim E. and Pourdeyhimi B. A study on compression-induced morphological changes of nonwoven fibrous materials, *Colloids and Surfaces A: Physicochemical and Engineering Aspects*, **337**(1–3), pp. 173–179, 2009.
101. Youssef S. Maire E. and Gaertner R. Finite element modelling of the actual structure of cellular materials determined by X-ray tomography, *Acta Mat.* **53**, pp. 719–730, 2005.
102. Rodal J. Soft nip calendering of paper and paperboard, *Tappi J.* **72**(5), pp. 177–189, 1989.
103. Kananen J. Rajatora H. and Niskanen K. Reversible compression of Sheet Structure, In **The Science of Papermaking**, *Trans. 12th Fund. Res. Symp. Oxford 2001* (C. F. Baker, ed.), pp. 1043–1066, FRC. Manchester, 2001.

104. Uesaka T. General formula for hygroexpansion of paper, *Journal of Material Science*, pp. 2373–2377, 1994.
105. Antoine C. Nygard P. Gregersen O. Holmstad R. Weitkamp T. and Rau C. 3D images of paper obtained by phase contrast X-Ray microtomography: image quality and binarisation, *Nuclear Instrument and Methods in Physics Research A*, **490**, pp. 392–402, 2002.
106. du Roscoat S. R. Bloch J. F. and Thibault X. Synchrotron radiation microtomography applied to investigation of paper, *J. of Physics D-Applied Physics*, **38**(10A, Sp. Iss. SI), pp. A78-A84, 2005.
107. Niskanen K. **Paper Physics**, Fapet Oy, Helsinki, Finland, 1998.
108. Belamaalem B. Contribution à l'étude de la structure du papier and de ses relations avec les propriétés physiques, PhD, Institut National Polytechnique de Grenoble, France, 1993.
109. Niskanen K. Dynamic hygroexpansion of paperboards, *Nordic Pulp and Paper Research Journal*, **12**(2), pp. 103–110, 1997.
110. Niskanen K. Nielsen N. Hellen E. and Alava M. KCL-PAKKA: Simulation of the 3 D structure of paper, Cambridge, UK, pp. 1273–1291, 1997.
111. Mercier C. Dubé M. Rolland du Roscoat, S. Bloch J. and Mangin P. Generalised 3-dimensional description of paper formation and structure, *Int. Paper Phys. Conf.* Golden Coast, Australia, pp. 81–86, 2007.
112. Decain M. Rolland du Roscoat, S. Bernard D. Geindreau C. and Bloch J. Détermination des propriétés microstructurales and physiques d'un matériau fibreux cellulosique à partir de microtomographies aux rayons X, *18*° Congrès Français de mécanique, Grenoble, France, 2007.

Transcription of Discussion

THREE-DIMENSIONAL STRUCTURAL ANALYSIS

Jean-Francis Bloch[1] and *Sabine Rolland du Roscoat*[2]

[1]G-INP/Pagora/LGP2/CNRS BP 65 F38402 Saint Martin d'Hères, France
[2]UJF/3S-R/CNRS, BP 53, F-38041, Grenoble Cedex 9, France

Ilya Vadeiko FPInnovations

I would like to thank you for showing some interesting pictures on the effect of relative humidity following yesterday's conversation. A quick question, you had a slide showing the correlation lengths for different directions (figures 11 and 12 in the paper in the proceedings, ed.). Could you open it again? You showed the correlation lengths in different directions so the question is: the x direction, is it MD or CD?

Jean-Francis Bloch

The first point is that it is the reason why I like to work with handsheets – because with handsheets there is no machine direction. And the second point is that if we really want to know exactly where the machine direction is, there are two ways of doing that. The first one, we usually put the sample with another paper sample. You make a mark in the MD, and by marking it, you are sure that you will find the machine direction. The second way is that you can also try to play with the images, and try to find what we call the main directions; the principle direction of your images. Then, you can say it corresponds to the machine direction.